ATTACHMENT (1)

CALVERT CLIFFS RESPONSE FOR RAI# E-3

Calvert Cliffs Nuclear Power Plant, LLC
April 24, 2013

ATTACHMENT (1)

CALVERT CLIFFS RESPONSE FOR RAI# E-3

REQUEST FOR ADDITIONAL INFORMATION (RAI)

E-3 *Provide justification for the acceptability of the storage of high burnup fuel (HBF) by providing analyses and an aging management program to demonstrate that HBF is protected against possible degradation that may lead to gross ruptures for storage periods beyond 20 years and potential operation safety problems during removal from storage.*

The requirements in 10 CFR 72.122(h) state that the spent fuel cladding must be protected during storage against degradation that leads to gross ruptures or the fuel must be otherwise confined such that degradation of the fuel during storage will not pose operational safety problems with respect to removal from storage. The analyses should address reasonable and known physical or degradation phenomena associated with storage periods from 20 to 60 years, such as cladding embrittlement due to precipitation of radial hydrides in HBF.

The aging management program should define specific confirmatory inspection or monitoring of stored HBF to address conflicting information, uncertainities, or indications of the presence of specific potential aging effects on the fuel. The program may specify inspection and monitoring of HBF within the cask system after 20 years of storage and at periodic intervals (e.g., every 10-20 years) during the renewal period; and may define an alternative, optional program to periodically review and use surrogate confirmatory information from other confirmation programs in the U.S. with similar HBF. The applicant may also consider proposing licensing conditions to limit the scope or storage time of HBF during the renewal period to address uncertainties and lack of confirmatory data.

This information is needed to evaluate compliance with 10 CFR 72.122(h).

CALVERT CLIFFS RESPONSE E-3:

Calvert Cliffs proposes to take a two pronged approach to aging management of high burnup fuel (HBF). The first would involve credit for a surrogate HBF aging management program that would be a joint effort between U.S. Department of Energy (DOE) and industry to inspect HBF in dry storage. The second would involve a demonstration that the fuel presently in storage at Calvert Cliffs either does not meet the definition of HBF or retained substantial margin, during the loading, transfer, and storage of the dry shielded canister (DSC), to the conditions which create special concerns for aging of HBF (principally the embrittlement of cladding by radially oriented zirconium hydrides). The former is intended to be the primary aging management program, while the latter provides additional assurance that fuel currently in storage is at low risk of suffering from aging mechanisms associated with HBF during the additional time that will be required for the DOE program to conduct the first HBF inspection.

Surrogate Aging Management Program

Due to the fact that the NUHOMS® DSCs in use at the Calvert Cliffs Independent Spent Fuel Storage Installation (ISFSI) are uninstrumented and utilize a welded closure method, there is no practical method to sample the interior fill gas or inspect the fuel being stored. Therefore, Calvert Cliffs intends to rely on the option of a surrogate program discussed above. The DOE has recently initiated procurement activities (DOE Solicitation #DE-SOL-00056019 – High Burnup Fuel Cask Research and Development) in support of a HBF aging management program which can be used as a surrogate program for industry. As described in Reference 1-1, we anticipate that the HBF demonstration project will be similar to the previous Dry Storage Characterization project for low burnup fuel discussed in Section 3.1.3 of our ISFSI License Renewal Application (Reference 1-2), except that this demonstration cask will be specially instrumented in advance so that data collection can begin as soon as the cask is loaded. After a period in

storage, plans call for opening the demonstration cask and examining the HBF. The proposed project is expected to consist of the following elements:

- Develop a detailed program plan/design and obtain necessary Nuclear Regulatory Commission (NRC) approvals
- Load well characterized used HBF of multiple cladding types into an existing bolted storage cask at a reactor site other than Calvert Cliffs
- Use a specially instrumented lid, to begin collecting data on temperature, moisture content, and internal gas composition immediately
- Perform hot cell examinations of "sister" rods, taken from the same HBF but not placed in dry storage, for baseline comparison
- After ten years or longer in storage, open the cask to perform visual and physical tests on the stored HBF.

This demonstration project is anticipated to yield significant relevant data prior to the point at which the HBF at Calvert Cliffs exceeds 20 years of dry storage (additional details on the timing of loading HBF at Calvert Cliffs is provided below).

On April 16, 2013 DOE awarded this contract to an Electric Power Research Institute (EPRI) team. Calvert Cliffs directly supports EPRI through our financial support of that organization and is an active participant on the steering committee for the team which prepared the bid. This will ensure Calvert Cliffs has input on the direction of the project and will be able to apply information learned from this project to the aging management program for HBF stored at Calvert Cliffs.

Expectation of Low Risk of HBF Aging Effects in Fuel Currently in Storage

Section 3.1.3 of the Calvert Cliffs ISFSI License Renewal Application (Reference 1-2) reviewed the aging mechanisms for fuel assemblies and identified hydrogen embrittlement and radial hydride formation as possible degradation mechanisms for HBF. The evaluation of fuel currently in storage for susceptibility to these mechanisms can be subdivided between fuel stored in 24P DSCs and fuel stored in 32P DSCs. Figure 1-1 provides the burnup distribution of fuel stored in the 48 loaded 24P DSCs at Calvert Cliffs. NUREG-1536 (Reference 1-3) defines HBF as "Spent nuclear fuel with burnups generally exceeding 45 GWd/MTU." As can be seen from Figure 1-1, the majority (99.7%) of fuel assemblies loaded in the 24P DSCs have burnups below 45 GWd/MTU, and would therefore be considered low burnup fuel. The four assemblies which have burnups above 45 GWd/MTU, exceed this value by only 0.09 to 0.82 GWd/MTU, and can essentially be considered low burnup fuel as well. Interim Staff Guidance (ISG)-11 Revision 3 (Reference 1-4) indicates that "*based on staff's evaluation, it is expected that fuel assemblies with burnups less than 45 GWd/MTU are not likely to have a significant amount of hydride reorientation due to limited hydride content. Further, most of the low burnup fuel has hoop stresses below 90 MPa. Even if hydride reorientation occurred during storage, the network of reoriented hydrides is not expected to be extensive enough in low burnup fuel to cause fuel rod failures.*" Based on this, the fuel stored in 24P DSCs is considered to not be at significant risk from the aging management concerns associated with extended storage of HBF. The 24 loaded 32P DSCs do however contain significant amounts of fuel that fall into the lower range of the HBF category. As can be seen in Figure 1-2, ~49% of the fuel stored in the 32P DSCs exceeds 45 GWd/MTU, and every DSC contains at least one assembly in this range. However, 98.7% of the fuel in the 32P DSCs has a burnup less than 49 GWd/MTU, and only one assembly exceeds 50 GWd/MTU (50.564 GWd/MTU specifically). No fuel exceeding 46.25 GWd/MTU was loaded prior to the September 2010 approval of License Amendment 9 which increased the burnup limit for the 32P DSC from 47 to 52 GWd/MTU.

The only guidance provided by the NRC on storage of HBF during the ISFSI license renewal period in NUREG-1927 (p. 20) (Reference 1-5) is as follows: "*The staff should assess whether the applicant has considered the most recent revision of ISG-11 and research results in this area, especially with respect to high-burnup fuel. Research into fuel performance in storage is ongoing. It is expected that the applicants would monitor these developments to ensure that they have identified potential degradation effects.*" On June 15, 2009, Calvert Cliffs submitted an analysis of fuel cladding temperatures (References 1-6 and 1-7) which demonstrated compliance with the requirements of ISG-11 Revision 3 (the most recent revision). On September 21, 2010, the NRC issued a safety evaluation report (Reference 1-8) which approved that analysis and indicated that "*loading operations will not result in repeated thermal cycling of the fuel, and the fuel will be maintained below 400°C during loading and storage, consistent with the guidance provided in ISG - 11, Revision 3.*" Interim Staff Guidance-11 Revision 3 indicates that the basis for the 400°C peak clad temperature (PCT) limit for all stages of ISFSI operation, and limitation on the number and magnitude of thermal cycles during the vacuum drying process, is to protect HBF cladding from aging mechanisms such as creep or embrittlement due to redissolution and precipitation of hydrides in a radial orientation. Table 1-1 below summarizes the design basis steady-state temperatures for a 32P DSC at the various stages of the loading, transfer, and storage processes, all of which show varying degrees of margin to the 400°C PCT limit.

Table 1-1, Design Basis 32P (0.66 kW/assembly; 21.12 kW/DSC) Peak Cladding Temperatures

Condition	Steady-State PCT
Vacuum Drying	742°F / 394°C (722°F at 110 hours)
Helium Backfill	536°F / 280°C
Transfer at -3°F Ambient	664°F / 351°C
Transfer at 103°F Ambient	742°F / 394°C
Storage at -3°F Ambient	545°F / 285°C
Storage at 70°F Ambient	597°F / 314°C
Storage at 103°F Ambient	620°F / 327°C

In practice, the actual 32P loadings at Calvert Cliffs have generally maintained substantial additional margin to the 400°C PCT limit due to less than design basis heat loads, milder ambient conditions than design basis, and the limited durations of the loading and transfer stages. An approximation of this additional margin can be made using loading records and thermal analysis information previously provided to the NRC for the Calvert Cliffs ISFSI. This estimate is made to assess margin only and is not intended to supplement the design basis thermal analyses for these DSCs. For each of the currently loaded DSCs at Calvert Cliffs, Table 1-2 summarizes heat loads at loading, and times when records indicate the various stages of the loading process were completed. The PCT during the blowdown and vacuum drying phase can easily be estimated using the time for this activity shown in Table 1-2 and the vacuum drying transient thermal analysis results from Reference 1-7, Table 7-1 for a 21.12 kW design basis 32P DSC (see Figure 1-3). That estimate which is also summarized in Table 1-2 indicates that PCTs during the blow down and vacuum drying range from 212 to 309°C. This estimate is conservative because it retains the assumption of a 21.12 kW heat load rather than the actual lower heat load of the 32P DSC being loaded.

Only the steady-state analyses at 21.12 kW discussed above were done for later stages of the 32P DSC loading and transfer process. However, steady-state analyses were performed for the 32PHB DSC in the Calvert Cliffs transfer cask (Reference 1-9) at various heat loads from 21.12 kW to 29.6 kW that can be used to estimate conservative PCTs for these stages as well. The primary physical difference between the current 32P and the proposed 32PHB DSCs is the solid aluminum rails at the periphery of the basket,

which help to improve hot transfer to the surface of the 32PHB DSC. Steady-state analyses for the 21.12 kW (uniform 660 W/assembly) heat load, show a fairly consistent ~6% higher PCT for 32P compared to 32PHB under near identical conditions. For example, Reference 1-10, Table 7-1 shows 704°F steady-state PCT during off-normal hot transfer operations (104°F ambient, 127 btu/hr-ft^2 insolation) for a 21.12 kW 32PHB while the current design basis 21.12 kW 32P has a steady-state PCT of 742°F for the same operation (analyzed at 103°F ambient, 127 btu/hr-ft^2 insolation). Similarly, the steady-state temperature of the 32P following helium backfill is 536°F, while the trend of steady-state 32PHB helium backfill temperatures (see Figure 1-4, plotted from Reference 1-11, Table 6-1) extrapolated down to a heat load of 21.12 kW yields 506°F, a difference of 6%. Therefore, the 32PHB linear trend was biased upward by 6% and used to extrapolate 32P steady-state helium backfill temperatures at lower heat loads using the fit shown in Figure 1-4. This linear extrapolation yields very conservative PCTs at lower heat loads since it predicts a 300°F PCT at 0 kW for 100°F ambient conditions. Applying this fit to the heat loads of the 24 loaded 32P DSCs shown in Table 1-2 yields helium backfill PCTs in the 222°C to 265°C range.

A similar approach was used to estimate the amount of margin to the 400°C limit for the 32P DSC transfers to the horizontal storage module (HSM) following draining of water from the annulus. For the transfer stage, only a steady-state calculation exists for the 32P DSC, and only transient calculations for different transfer times were performed for the 32PHB at various heat loads above 21.12 kW (References 1-11 and 1-12, Table 7-1 in both). However, this information can be used to calculate the cladding heat-up rate as a function of DSC heat load, since the steady-state helium backfill temperatures from Reference 1-10 were used as the starting point for the transfer transient analysis. The heat up rate for a given heat load, is simply the peak cladding temperature for transfer minus the helium backfill temperature, and divided by the maximum transfer time allowed for that heat load without forced cooling in Reference 1-11 or 1-12 (also in Table 7-1). The resulting 32PHB transfer heat-up rates are plotted in Figure 1-5. These were biased upward by 6% to account for basket differences between 32P and 32PHB, and fit to the exponential function shown in Figure 1-5. Transfer PCTs were then estimated for each 32P loading using this function and the DSC heat load to determine a heat-up rate, multiplying that rate by the transfer time, and adding it to the steady-state helium backfill PCT for that loading. This is expected to yield conservative PCTs given that, in addition to the conservatism discussed previously for the helium backfill PCT, the transfer heat-up rate fit is based on off-normal hot transfer cases, and the 32P in its transfer cask normally spends the majority of the transfer time shown in Table 1-2 sitting in a large climate controlled truck bay without solar insolation. The results indicate that the transfer PCTs for the majority of transfers range between 265°C and 341°C. For Loading 69 (DSC-67, which was loaded into HSM-45), an issue with the top shield plug top casing plate resulted in the transfer cask remaining in the truck bay for an off-normal duration. This 32P DSC likely achieved steady-state conditions, which in the absence of further detailed analysis, can only be confirmed to be less than the 394°C calculated for a design basis 32P given the lower heat load of Loading 69 and the milder conditions associated with its transfer.

Figure 1-6 summarizes the estimated margin to the ISG-11 Revision 3 limits for the currently loaded 32P DSCs. It is expected that 96% of the DSCs have maintained at least 50°C margin to this limit during the loading and transfer process, and over half have maintained greater than 100°C of margin. Note also that these PCTs represent only short-term conditions during loading/transfer and that margin for long-term storage is greater than 70°C even for a design basis heat load. The margin afforded by these lower PCTs in terms of the degree of radial hydride precipitation was evaluated in detail during the period 2000 to 2002 as a result of interactions between Nuclear Energy Institute, EPRI, and the NRC. These evaluations are compiled in Reference 1-13, and eventually were used as part of the supporting basis for the 400°C limit that first appeared in ISG-11 Revision 2. One of the principal developments of Reference 1-13 was a radial hydride precipitation model as a function of cladding hoop stress and PCT at the beginning of

storage. Reference 1-14 provides the latest analyses using that model, which are echoed in Table 1-3. As can be seen in Table 1-3, the concentration of radial hydrides for a given cladding hoop stress is a factor 4 times lower than the 400°C value with 50°C of margin, and almost a factor of 10 times lower with 100°C of margin. Even Loading 69 has likely retained at least a factor of 2 less radial hydrides than would be expected at 400°C. Thus, the estimated conditions of the actual loaded 32P DSCs support the expectation that the fuel they contain is at low risk of suffering from HBF related aging mechanisms. It is expected that the HBF surrogate aging management program discussed above will provide positive confirmation of this during the renewal period.

REFERENCES

1-1 Letter from R. McCullum (NEI) to M. Lombard (NRC), dated March 22, 2013, "Industry Analysis and Confirmatory Information Gathering Program to Support the Long-Term Storage of High Burnup Fuel (HBF)," ML13084A045

1-2 Letter from G. H. Gellrich (CCNPP) to Document Control Desk (NRC), dated September 17, 2010, Site-Specific Independent Spent Fuel Storage Installation (ISFSI) License Renewal Application

1-3 NUREG-1536, "Standard Review Plan for Spent Fuel Dry Storage Systems at a General License Facility," U.S. Nuclear Regulatory Commission, Revision 1, July 2010

1-4 Interim Staff Guidance 11, "Cladding Considerations for the Transportation and Storage of Spent Fuel," U.S. Nuclear Regulatory Commission, November 2003

1-5 NUREG-1927, "Standard Review Plan for Renewal of Spent Fuel Dry Cask Storage System Licenses and Certificates of Compliance," March 2011

1-6 Letter from J. A. Spina (CCNPP) to Document Control Desk (NRC), dated June 15, 2009, Calvert Cliffs Nuclear Power Plant, Independent Spent Fuel Storage Installation - License Amendment Request: Allow Increased Burnup fuel to be loaded into NUHOMS-32P Dry Shielded Canister, ML091680541

1-7 Transnuclear Calculation NUH32P+.0401, "Thermal Analysis of NUHOMS 32P+ DSC for Vacuum Drying Condition," ML091680551

1-8 Letter from J. Goshen (NRC) to G. H. Gellrich (CCNPP), dated September 14, 2010, Amendment 9 to Material License No. SNM-2505 for the Calvert Cliffs Independent Spent Fuel Storage Installation (TAC No. L24350), ML102571628

1-9 Letter from G. H. Gellrich (CCNPP) to Document Control Desk (NRC), dated December 8, 2011, License Amendment Request: High Burnup NUHOMS®-32PHB Dry Shielded Canister and Horizontal Storage Modules, ML12006A140

1-10 Transnuclear Calculation NUH32PHB-0406, "Thermal Evaluation of NUHOMS 32PHB Transfer Cask for Normal, Off Normal, and Accident Conditions (Heat Loads <29.6kW)," ML12093A103

1-11 Transnuclear Calculation NUH32PHB-0408, "Thermal Analysis of NUHOMS 32PHB DSC for Vacuum Drying Operations," ML12093A102

1-12 Transnuclear Calculation, NUH32PHB-0403, Rev. 0, "Thermal Evaluation of NUHOMS 32PHB DSC for Storage and Transfer Conditions," ML12173A182

1-13 Electric Power Research Institute Report 1009276, "Dry Storage of High-Burnup Spent Fuel - Responses to Nuclear Regulatory Commission Requests for Additional Information and Clarification," November 2003

1-14 Electric Power Research Institute Report 1015048, "Spent Fuel Transportation Applications-Assessment of Cladding Performance: A Synthesis Report," December 2007

Table 1-2, Estimate of Peak Cladding Temperatures for Currently Loaded 32P Canisters During the Loading and Transfer Process

Loading	32P DSC Heat Load at Loading (kW)	Blowdown Start Time (Note 5)	Completion of Dryness Test	Blowdown & Vacuum Drying Time (hours)	PCT During Blowdown & Vacuum Drying (see Note 1)		PCT Following Helium Backfill (see Note 2)		Annulus drained (Note 6)	HSM insertion (Note 7)	Transfer Time (hours)	Transfer PCT (see Note 3)	
					°F	°C	°F	°C				°F	°C
49	16.12	11/25/2005 10:00	11/27/2005 5:15	43.3	587	309	482	250	11/29/2005 6:00	11/30/2005 15:00	33	512	267
50	15.85	1/17/2006 15:15	1/18/2006 15:06	23.9	470	243	479	248	1/21/2006 4:00	1/24/2006 14:27	82	551	288
51	15.26	8/22/2006 17:30	8/24/2006 1:40	32.2	528	276	472	245	8/25/2006 5:00	8/28/2006 12:45	80	536	280
52	17.43	9/12/2006 22:35	9/14/2006 3:04	28.5	504	262	496	258	9/14/2006 18:00	9/18/2006 12:45	91	597	314
53	14.70	1/9/2007 20:20	1/10/2007 21:40	25.3	481	250	466	241	1/11/2007 21:30	1/15/2007 12:30	87	530	277
54	14.07	5/16/2007 13:47	5/17/2007 16:13	26.4	489	254	459	237	5/18/2007 21:00	5/21/2007 10:45	62	501	260
55	14.55	6/5/2007 7:15	6/6/2007 4:51	21.6	452	233	465	240	6/7/2007 9:00	6/11/2007 11:45	99	536	280
56	14.67	11/13/2007 10:30	11/14/2007 11:05	24.6	475	246	466	241	11/15/2007 9:30	11/19/2007 12:05	99	538	281
57	11.76	8/19/2008 22:25	8/21/2008 14:50	40.4	574	301	434	223	8/22/2008 22:30	8/25/2008 11:30	61	463	239
58	13.65	9/3/2008 17:00	9/4/2008 14:52	21.9	454	234	455	235	9/5/2008 15:00	9/8/2008 9:35	67	497	258
59	12.64	9/16/2008 3:00	9/17/2008 1:50	22.8	462	239	444	229	9/17/2008 22:10	9/22/2008 9:45	108	502	261
60	11.53	9/30/2008 13:55	10/1/2008 15:20	25.4	482	250	432	222	10/2/2008 12:00	10/6/2008 9:15	93	474	246
61	14.70	8/18/2009 15:12	8/19/2009 10:25	19.2	432	222	466	241	8/20/2009 12:00	8/24/2009 12:15	96	537	281
62	16.97	9/2/2009 8:10	9/3/2009 2:30	18.3	424	218	491	255	9/4/2009 11:00	9/9/2009 10:20	119	615	324
63	15.44	9/15/2009 10:50	9/16/2009 5:25	18.6	427	219	474	246	9/17/2009 3:30	9/21/2009 9:45	102	558	292
64	18.35	10/5/2010 17:00	10/6/2010 22:00	29.0	507	264	506	263	10/7/2010 20:30	10/11/2010 12:50	88	619	326
65	17.88	10/20/2010 10:15	10/21/2010 9:10	22.9	462	239	501	260	10/22/2010 16:00	10/25/2010 10:45	67	580	305
66	18.62	11/2/2010 18:00	11/3/2010 16:15	22.3	457	236	509	265	11/5/2010 0:30	11/8/2010 11:40	83	620	327
67	16.35	8/11/2011 4:35	8/11/2011 22:30	17.9	421	216	484	251	8/13/2011 0:15	8/16/2011 10:15	82	562	294
68	17.94	8/23/2011 16:30	8/24/2011 10:45	18.2	424	218	501	261	8/25/2011 13:00	8/30/2011 13:15	120	646	341
69	18.30	9/13/2011 9:30	9/14/2011 3:50	18.3	424	218	505	263	9/27/2011 14:30	10/6/2011 10:30	212	<742[4]	<394[4]
70	18.60	8/21/2012 16:20	8/23/2012 1:00	32.7	531	277	509	265	8/24/2012 10:00	8/28/2012 11:30	98	639	337

Table 1-2, Estimate of Peak Cladding Temperatures for Currently Loaded 32P Canisters During the Loading and Transfer Process

Loading	32P DSC Heat Load at Loading (kW)	Blowdown Start Time (Note 5)	Completion of Dryness Test	Blowdown & Vacuum Drying Time (hours)	PCT During Blowdown & Vacuum Drying (see Note 1)		PCT Following Helium Backfill (see Note 2)		Annulus drained (Note 6)	HSM insertion (Note 7)	Transfer Time (hours)	Transfer PCT (see Note 3)	
					°F	°C	°F	°C				°F	°C
71	18.57	9/11/2012 13:50	9/12/2012 7:44	17.9	421	216	508	265	9/13/2012 9:00	9/17/2012 11:00	98	638	337
72	17.22	9/25/2012 9:52	9/26/2012 3:00	17.1	414	212	494	256	9/27/2012 5:00	10/1/2012 10:00	101	603	317

Note 1 PCT is calculated by inputting the blowdown and vacuum drying time into the fit shown in Figure 1-3 (all temperatures are based on 21.12 kW DSC heat load).

Note 2 Helium Backfill PCT is calculated by inputting the DSC heat load in kW into the fit shown in Figure 1-4.

Note 3 Transfer PCT is calculated by inputting the DSC heat load in kW into the fit shown in Figure 1-5, multiplying the resulting rate by the transfer time, and adding to the Helium backfill PCT.

Note 4 Due to the extended transfer time, PCT can only be determined to be less than the steady-state hot transfer PCT for a 21.12 kW 32P DSC.

Note 5 If a specific time was not recorded for start of blowdown, the blowdown start time was taken to be the time recorded for removal of the hydrogen monitor following completion of top shield plug welding.

Note 6 Annulus drain time based on time noted on radiation surveys taken immediately following draining or time indicated on annulus water sample collected at time of draining.

Note 7 HSM insertion time taken to be 2 hours prior to the time listed for the initial HSM delta-T surveillance, which occurs 1 hour after installation of HSM door.

Table 1-3, Radial Hydride Concentration (ppm) as a Function of Beginning of Storage Temperature and Hoop Stress (Reference 1-14, Table 2-2)

Hoop Stress (MPa)	Temperature (°C)									
	410	400	390	380	370	360	350	340	330	320
200	29.1	21.6	16.0	11.7	8.6	6.3	4.6	3.4	2.5	1.8
190	23.6	17.4	12.9	9.5	7.0	5.1	3.8	2.8	2.0	1.5
180	19.0	14.1	10.4	7.7	5.7	4.2	3.1	2.3	1.7	1.2
170	15.3	11.4	8.4	6.3	4.6	3.4	2.5	1.9	1.4	1.0
160	12.4	9.2	6.9	5.1	3.8	2.8	2.1	1.6	1.2	0.9
150	10.0	7.4	5.6	4.1	3.1	2.3	1.7	1.3	1.0	0.7
140	8.0	6.0	4.5	3.4	2.5	1.9	1.4	1.1	0.8	0.6
130	6.5	4.9	3.7	2.7	2.1	1.5	1.2	0.9	0.7	0.5
120	5.2	3.9	2.9	2.2	1.7	1.3	1.0	0.7	0.5	0.4
110	4.1	3.1	2.4	1.8	1.3	1.0	0.8	0.6	0.4	0.3
100	2.7	2.1	1.6	1.2	0.9	0.7	0.5	0.4	0.3	0.2
90	2.1	1.6	1.2	0.9	0.7	0.5	0.4	0.3	0.2	0.2
80	1.4	1.1	0.8	0.7	0.5	0.4	0.3	0.2	0.2	0.1
70	0.9	0.7	0.6	0.4	0.3	0.3	0.2	0.2	0.1	0.1
60	0.6	0.5	0.4	0.3	0.2	0.2	0.1	0.1	0.1	0.1

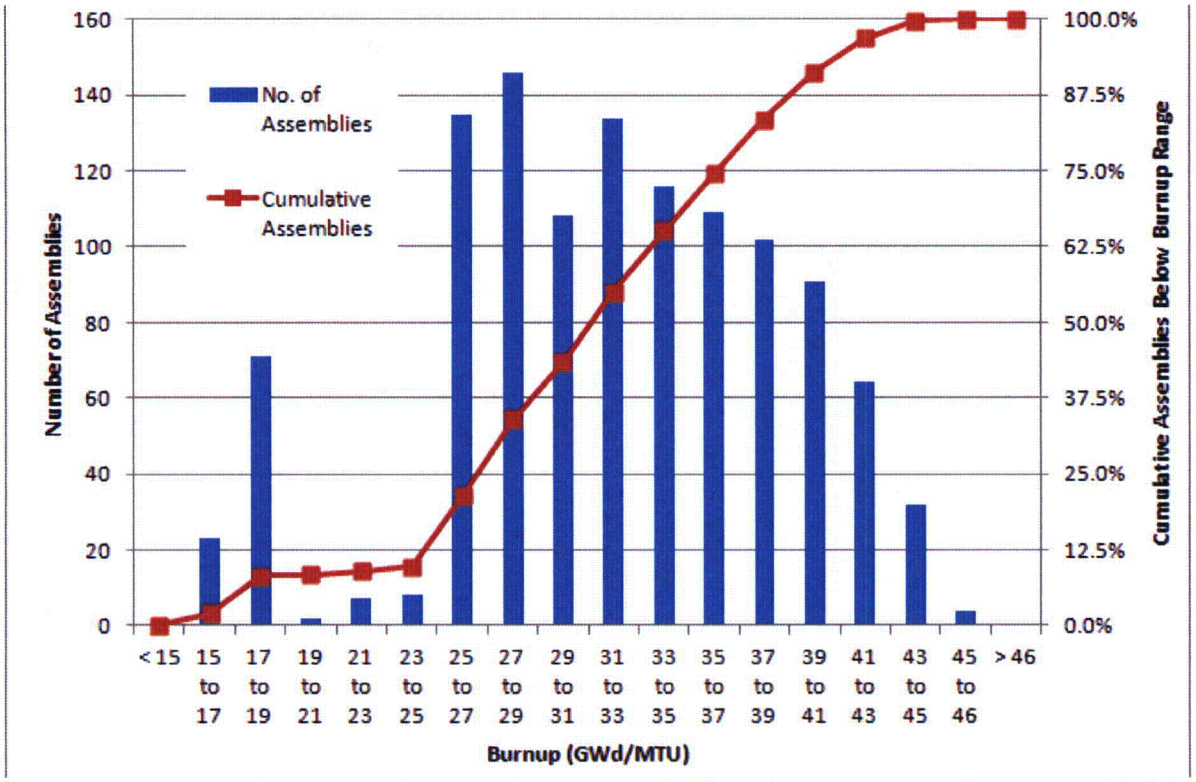

Figure 1-1 - Assembly Average Burnup Distribution of Fuel Stored in the 48 Loaded 24P DSCs

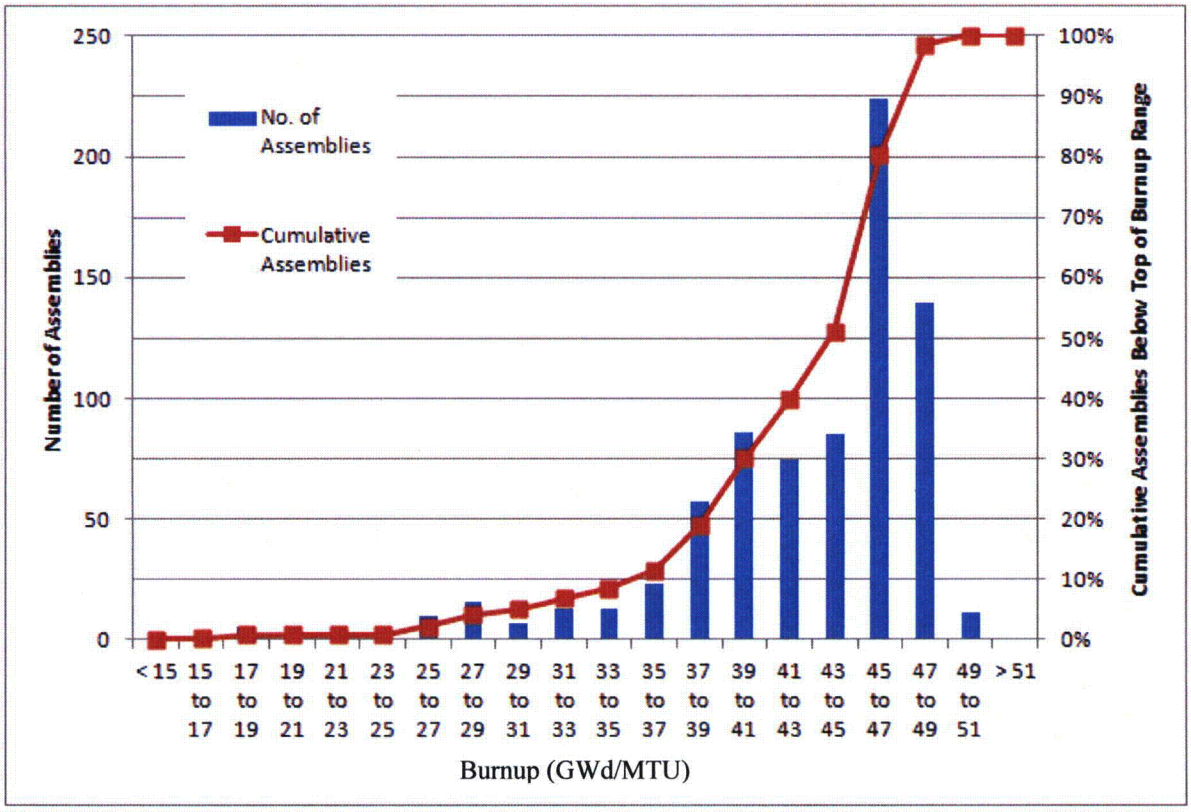

Figure 1-2 - Assembly Average Burnup Distribution of Fuel Stored in the 24 Loaded 32P DSCs

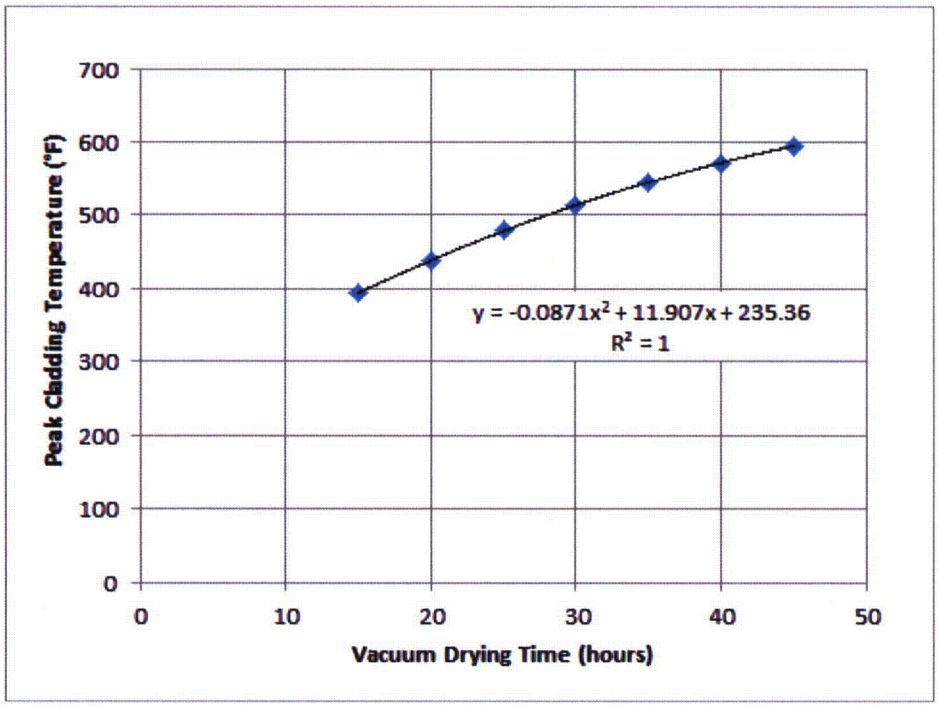

Figure 1-3 - 32P Design Basis (21.12 kW) Vacuum Drying Transient Thermal Analysis Results (plotted for the range of interest from Reference 1-7, Table 7-1)

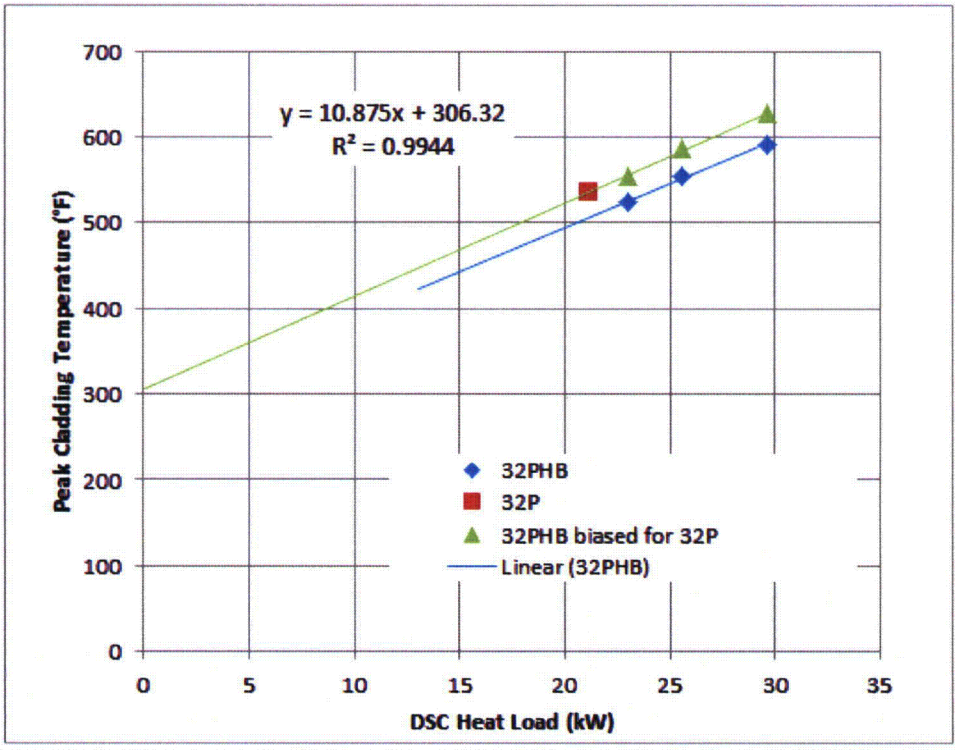

Figure 1-4 - Steady-state Helium Backfill PCTs as a Function of DSC Heat Load (32PHB temperatures plotted from Reference 1-11, Table 6-1)

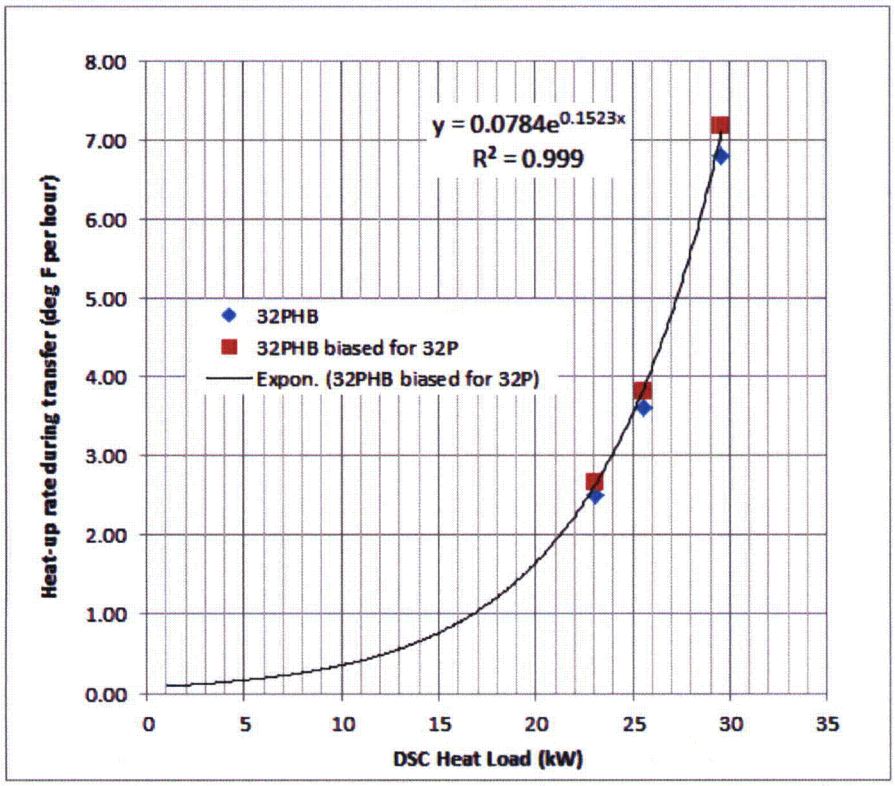

Figure 1-5 - Estimated Cladding Heat-Up Rate During Off-Normal Hot Transfer as a Function of DSC Heat Load (based on information in Reference 1-11 Table 6-1)

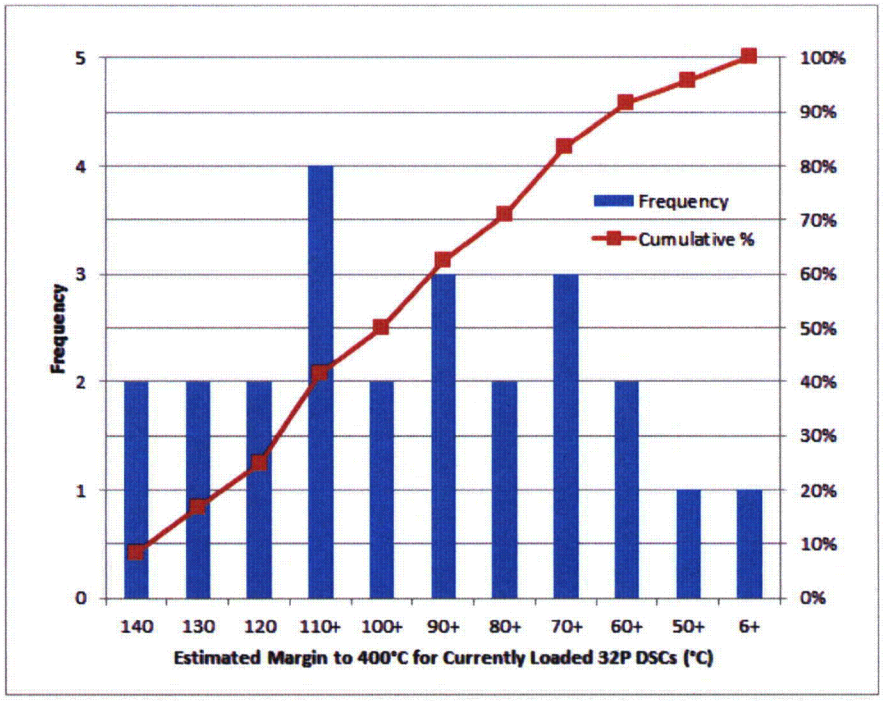

Figure 1-6 - Summary of Estimated Margin to ISG-11 Limits for HBF PCT During the Loading and Transfer Process

ATTACHMENT (2)

COLLECTION AND ANALYSIS OF SURFACE DEPOSITS FROM A CALVERT CLIFFS DSC

Calvert Cliffs Nuclear Power Plant, LLC
April 24, 2013

ATTACHMENT (2)

COLLECTION AND ANALYSIS OF SURFACE DEPOSITS FROM A CALVERT CLIFFS DSC

Collection and Analysis of Surface Deposits from a Dry Shielded Canister (DSC) at the Calvert Cliffs Independent Spent Fuel Storage Installation

As discussed briefly in Reference 2-1, the inspection performed on DSC-11 in horizontal storage module-1 in June 2012 included collection of samples of the material deposited on the DSC surface (DSC-11 was the first DSC placed into storage in November 1993) as part of the Electric Power Research Institute sponsored inspection scope. Samples were collected using both a wet and a dry method.

The dry method used a tool consisting of an abrasive type sponge (Scotch-Brite™) with filter paper on a removable cartridge mounted at the end of a long handled tool with vacuum applied to ensure sample retention (see Figure 2-1). The tool head was rotated away from the side of the DSC, inserted in the horizontal storage module along the side of the DSC, rotated to make contact with the DSC surface, then scrapped back and forth several times to collect the loose dust and debris (length of stroke was 15.24 cm and width of sponge/filter was 2.54 cm). Three dry samples from the DSC shell were located at different radial locations and axial locations from the bottom of the DSC: 1) at the 11 o'clock position (oriented with the bottom of the DSC as the "clock face") ~100 cm in from the bottom, 2) at the 7 o'clock position ~100 cm in from the bottom, and 3) at the 3 o'clock position near the bottom edge of the DSC. Once the scraper samples were collected, the cartridges were placed in individual bags for storage for future chemical analysis. The laboratory analysis results for the samples taken at the 3 o'clock position are included as Enclosure 1. The analyses performed include: 1) X-ray Diffraction for quantitative phase identification, 2) X-ray Fluorescence for a semi-quantitave elemental analysis, 3) Gas Chromatography Mass Spectrometry for identifying volatile and semi-volatile materials, and 4) Ion Chromatography to identify major cations and anions. Electric Power Research Institute has retained the other two scraper cartridges for further analyses at a national laboratory later this year.

The wet method used a commercially available device (SaltSmart™) which measures the salt concentration by dissolving the salt on the surface, measuring the conductivity and determining the concentration based on a calibration of the device. The device was calibrated for a range of 0 to 1 g/m^2 of sea salt deposited on 304 SS (Morton brand grocery store sea salt from the Pacific Ocean). The device was inserted using a specially developed tool that deployed the device to the desired area (see Figure 2-1), applied it to the surface of the DSC shell, injected the water to dissolve the salt on the surface, and then withdrew the device for reading. The measurement was performed at one location on DSC-11, at the 11 o'clock position near the bottom edge of the DSC. After the conductivity based measurement was read, the used device was stored for later separate analysis. That analysis is also included in Enclosure 1, and consisted of the same scope of tests performed for the scraper tool.

The only salt concentration measurement completed at the time of the inspection was the conductivity based reading from the SaltSmart™ device, which indicated 0.5 g/m^2 salt. Based on the laboratory analyses in Enclosure 1, this conductivity based measurement is now believed by Electric Power Research Institute and the SaltSmart manufacturer to be invalid in the high direction. SaltSmart™ devices measure the fully combined conductivity of the sum total of all salts and free ions present in the solution created in the extraction process. SaltSmart™ does not differentiate between types of salts or ions. Nitrate salts and sulfates also contribute to the conductivity and are measured as well, in the total salt solution. The ion chromatography report in Enclosure 1 specifically notes that sulfates were present in much higher concentrations than chlorides. This pattern is also evident in the chemical composition of rainwater collected at the National Atmospheric Deposition Program, Wye, MD site that is north of Calvert Cliffs on the opposite side of the Chesapeake Bay as noted in Table 2-1 of Reference 2-2. In contrast, sulfates are generally present in much lower concentration compared to sodium and chlorides in sea salt (Reference 2-3). Thus, since the SaltSmart™ was not calibrated with a mixture similar in composition to that actually found on the DSC, and much of the conductivity being measured could occur

from sources other than sea salt, the conductivity based result from last summer has been deemed unreliable. The actual laboratory analysis of the concentration of chlorides on the SaltSmart™ and scraper in Enclosure 1 are considered a more accurate measurement of the chlorides present on DSC-11 after almost 19 years of storage. The highest concentration of chloride obtained from x-ray fluorescence of the SaltSmart™ was found to be 5.2 mg/m^2.

REFERENCES

2-1 Letter from G. H. Gellrich (CCNPP) to Document Control Desk (NRC), dated July 27, 2012, Response to Request for Supplemental Information, RE: Calvert Cliffs Independent Spent Fuel Storage Installation License Renewal Application (TAC No- L24475), ML12212A216

2-2 Electric Power Research Institute Report 1013524, "Climactic Corrosion Considerations for Independent Spent Fuel Storage Installations in Marine Environments," June 2006

2-3 M. J. Atkinson and C. Bingman, "Elemental Composition of Commercial Seasalts," Journal of Aquariculture and Aquatic Sciences, Volume VIII, No. 2

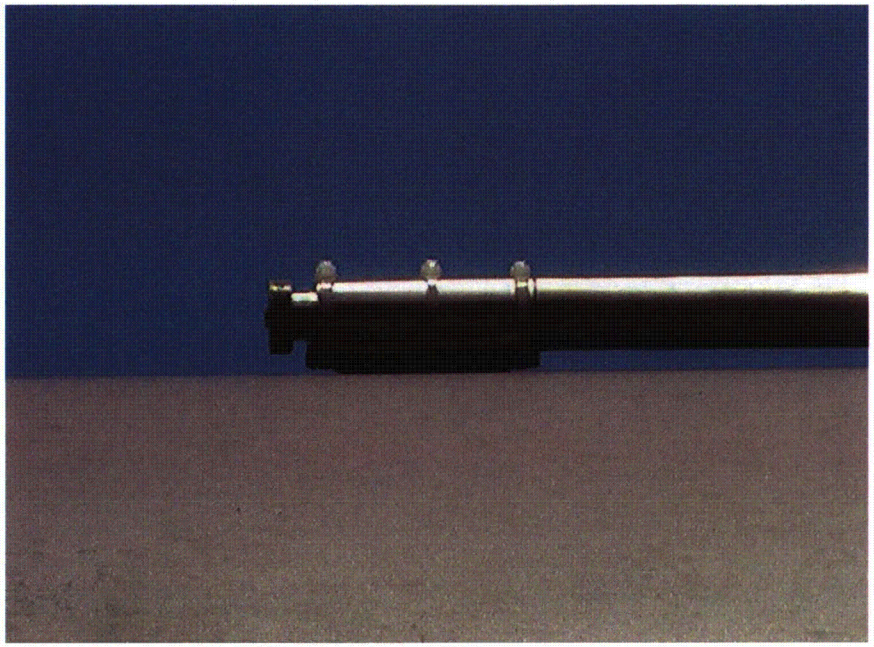

Scraper (Dry) Tool

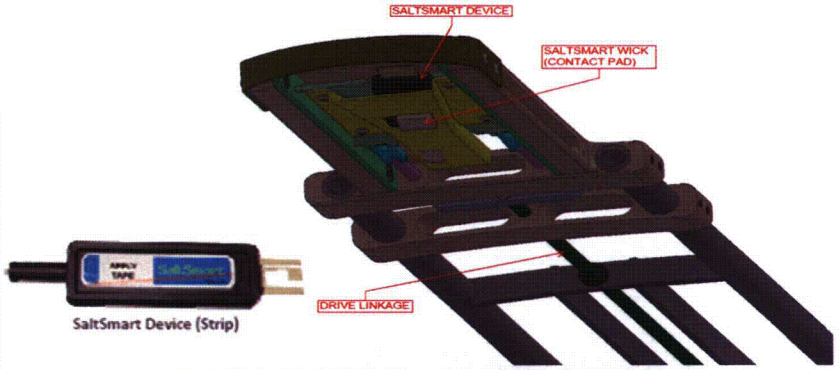

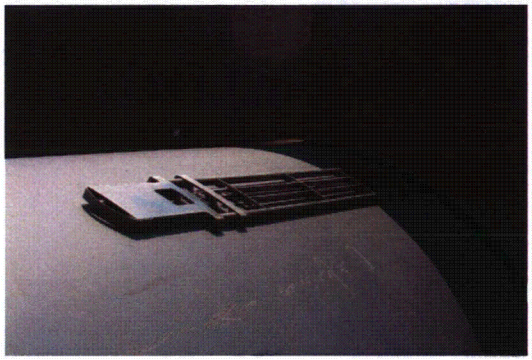

Photo courtesy of Transnuclear

SaltSmart (Wet) Tool

Figure 2-1, DSC Surface Sampling Tooling (deployed on mock-up)

ENCLOSURE 1

EPRI Chemical Analysis Results

Calvert Cliffs Nuclear Power Plant, LLC
April 24, 2013

EPRI | ELECTRIC POWER RESEARCH INSTITUTE

March 25, 2013

Ron Seagraves
Calvert Cliffs Nuclear Power Plant
NOF-2
1650 Calvert Cliffs Parkway
Lusby, MD 20657

Subject: Calvert Cliffs Canister Inspection Chemical Analysis Results of Samples Collected

Dear Mr. Seagraves:

During the canister inspection at Calvert Cliffs Nuclear Power Plant in June 2012, a total of four surface samples were collected from DSC-11 in HSM-1; three using the scraper tool cartridge and one using a SaltSmart™ device. A set of analyses have been completed on one scraper sample (#3 taken from the 3 o'clock position at the edge) and the single SaltSmart™ sample (taken at the 9 o'clock position fully inserted). The analyses performed include: 1) X-ray Diffraction (XRD) for a quantitative phase identification, 2) X-ray Fluorescence (XRF) for a semi-quantitative elemental analysis, 3) Gas Chromatography Mass Spectrometry (GCMS) for identifying volatile and semi-volatile materials, and 4) Ion Chromatography to identify major cations and anions. For each analysis, six samples were tested: the Scotch-Brite™ from Scraper Sample #3, the filter paper from Scraper Sample #3, the used SaltSmart™, an unused Scotch-Brite™ sample, an unused filter paper, and an unused SaltSmart™. Included in Attachment 1 is a summary of the concentrations from the used filter and SaltSmart™. Attachments 2 through 5 are the completed lab analysis reports for the samples analyzed.

The remaining two scraper samples are to be analyzed separately. We are working with a national laboratory to get an agreement in place for this analysis which will provide more detail and characterization of the material from these dry samples that were collected. We will transmit those results separately when they become available.

If you have any questions, please contact me at (704) 595-2887 or kwaldrop@epri.com.

Sincerely,

Keith Waldrop
Senior Project Manager

074646

CHARLOTTE OFFICE
1300 West W.T. Harris Boulevard, Charlotte, NC 28262-8550 USA • 704.595.2000 • Fax 704.595.2860
Customer Service 800.313.3774 • www.epri.com

Attachments 1 - 5

c: John Kessler
John Massari (CCNP)
Philip Wengloski (CCNP)

ATTACHMENT 1

Summary of Concentrations from X-Ray Fluorescence[1]

	Filter Used[2] (mg/m2)	SaltSmart Used (mg/m2)
O	-[3]	161
Na	0.33	5
Mg	1.2	13.9
Al	3.7	27.7
Si	13	134
P	0.76	5.9
S	3.4	12
Cl	-	5.2
K	13	48.4
Ca	67	463
Ti	-[4]	23.4
Cr	215	3.1
Mn	29.1	8.0
Fe	1077	256
Ni	102	2
Cu	6.0	-
Zn	17.4	34.3
Zr	-	2.0

[1] – Determined from the total areal density of the residue on the filter surface and a compositional breakdown of the residue in weight percent.

[2] – The area considered for the concentration from the filter only includes the area of the filter analyzed and does not account for the area covered in the back and forth scraping motion.

[3] – Oxygen is likely present in the residue as one or more metal oxides; however, it cannot be quantified due to the high O content in the filter.

[4] – Titanium appears to be present in the residue from this sample; however, it cannot be quantified due to the presence of Ti in the filter itself.

ATTACHMENT 2

X-ray Diffraction
Phase Identification

ISO 17025

Testing Cert. #2797.01

X-RAY DIFFRACTION (XRD) ANALYSIS REPORT 21 Mar 2013

JOB NUMBER C0DHY160 PO NUMBER 4500000443

for

Keith Waldrop
Electric Power Research Institute

Prepared by:

Wes Nieveen
Scientific Fellow
(Tel. 408-530-3756; wnieveen@eaglabs.com)

Reviewed by:

Stephen B. Robie, Ph.D.
Specialist, XRD Services
(Tel. 408-530-3638; srobie@eaglabs.com)

Evans Analytical Group
810 Kifer Rd
Sunnyvale, CA 94086 USA

Requester: Keith Waldrop
Job Number: C0DHY160
Analysis Date: 21 Mar 2013

X-RAY DIFFRACTION ANALYSIS REPORT

Purpose: Use XRD to identify and quantify the possible crystalline phases present on several collection devices/materials used to collect dust from storage canisters. The samples are labeled and referred to as; SaltSmart Used, SaltSmart Control, Scotch-Brite Used, Scotch-Brite Control, Filter Paper Used, and Filter Paper Control

Summary: Quantification of the samples was not possible for several reasons; not all phases were identified, more than one amorphous phase was present, some database references did not extend to high enough 2-Theta angles, and some phases do not have RIR (relative intensity ratios) required for quantification.

Table 1: Phase Identification Results for Smart Salt Control and Used.*

Sample	Phases present
Salt Smart Control	$(C_3H_6)_n$; Polypropylene Monoclinic PDF#00-054-1936 $(C_2H_4)_n$; Polyethylene Monoclinic , C2/m PDF#00-054-1981 $(C_3H_6)_n$; α-Polypropylene Monoclinic , P21/c PDF#00-061-1416 Possibly; $((C_{10}H_8O_4)_{0.90}(C_{10}H_{14}O_4)_{0.10})_n$; Poly(ethylene terephthalate-co-1,4-cyclohexane dicarboxylate) Triclinic PDF#00-058-1449

Sample	Phases present
Salt Smart Used **(Phases listed above plus these additional phases)**	$Mg_2Al_4Si_5O_{18}$; Magnesium Aluminum Silicate Orthorhombic PDF#00-060-0061 $NaSi_{33}O_{66.5}{\cdot}x\ H_2O$; Sodium Silicate Hydrate Orthorhombic PDF#00-049-0673 SiO_2; Quartz, Silicon Oxide Hexagonal , P3221 PDF#00-046-1045 $Al(OH)_3$; Gibbsite (Aluminum Hydroxide) Monoclinic , P21/n PDF#00-007-0324 MgO; Periclase, syn (Magnesium Oxide) Cubic , Fm-3m PDF#00-004-0829 $CaCO_3$; Calcite, Calcium Carbonate Rhombohedral , R-3c PDF#00-005-0586 $CaMg(CO_3)_2$; Dolomite (Calcium Magnesium Carbonate) Rhombohedral, R-3 PDF#00-011-0078

Table 2: Phase Identification Results for Scotch Brite Control and Used.*

Sample	Phases present
Scotch Brite Control	AlN; Aluminum Nitride Cubic, Fm-3m PDF#00-046-1200 Al_2O_3; Corundum, syn (Aluminum Oxide) Rhombohedral, R-3c PDF#00-010-0173 Unknown phase(s)
Scotch Brite Used	AlN; Aluminum Nitride Cubic, Fm-3m PDF#00-046-1200 Al_2O_3; Corundum, syn (Aluminum Oxide) Rhombohedral, R-3c PDF#00-010-0173 Unknown phase(s)

Table 3: Phase Identification Results for Filter Paper Control and Used.*

Sample	Phases present
Filter paper Control	$(C_{10}H_8O_4)_n$; Polyethylene terephthalate (PET) Triclinic, P-1 PDF#00-060-0989 Unknown phase(s)

Sample	Phases present
Filter paper Used	$(C_{10}H_8O_4)_n$; Polyethylene terephthalate (PET) Triclinic, P-1 PDF#00-060-0989 $CaMg(CO_3)_2$; Dolomite (Calcium Magnesium Carbonate) Rhombohedral, R-3 PDF#00-011-0078 $Fe^{+2}Fe_2^{+3}O_4$; Magnetite, syn (Iron Oxide) Cubic, Fd-3m PDF#00-019-0629 MgO; Periclase, syn (Magnesium Oxide) Cubic , Fm-3m PDF#00-004-0829 $CaCO_3$; Calcite, Calcium Carbonate Rhombohedral , R-3c PDF#00-005-0586 SiO_2; Quartz, Silicon Oxide Hexagonal , P3221 PDF#00-046-1045 Unknown phase(s)

Discussion and Results: XRD data for the Scotch Brite samples were acquired by coupled Theta:2-Theta scans on a PANalytical X'Pert Pro MRD diffractometer equipped with a Copper x-ray tube and parallel-beam optics. Data for the Salt Smart and Filter paper samples were acquired on a Bruker GADDS microdiffractometer equipped with a copper x-ray tube, incident-beam monochromator, 500micron pinhole collimator, laser alignment system and 2D detector. Unlike traditional point detectors, the 2D detector accepts diffraction from crystallites oriented in a wide variety of tilt angles with respect to the incident x-ray beam. This results in reasonable diffraction intensity even though the spot size analyzed is very small. Because the

areas of interest on some of the collection material were irregular and inhomogeneous, the use of the smaller spot GADDS system provides better information and signal-to-noise than the other larger area XRD systems. The SmartSalt samples were initially analyzed as-received on the device, complete and intact. However, the x-ray penetration depth extended quite some distance (several mm's) into the underlying backing foam on the devices. These samples were also analyzed in transmission mode after the top collection surface material was removed for XRF analysis.

Photo 1 and Photo 3 show the low magnification images of the SmartSalt Control and Used samples on the complete and intact device. Photo 2 and Photo 4 show the high magnification images from the alignment camera for the SmartSalt Control and SmartSalt Used samples respectively. The darkened area on the SmartSalt Used sample is the location of particles and dust collected by the device. On two of the alignment photos, the laser spot located at the crosshairs can also be observed.

Figure 1 and Figure 3 show the frames from the 2-D detector acquired at 2-Theta angles of 22°, 42°, 62°, and 82° for the SmartSalt Control and SmartSalt Used sample respectively. 2-Theta increases from right to left across each frame. Each arc in the 2D image corresponds to a single d-spacing. Each position along the arc is a different tilt angle. The 2D image covers about 32 degrees 2-Theta so there is considerable overlap from one frame to the next. Some of the arcs are continuous but do not extend complete from top to bottom of the frame. Some arcs are continuous but with bright spots on the arc. The bright spots correspond to larger grains or more grains oriented in the same direction. Some arcs are only a few spots and this corresponds to a few large grained crystallites. Note that the low angle frames also have a broad, wide, diffuse arc/band from top to bottom superimposed on the more distinct arcs. These wide bands are due to amorphous (non-crystalline material) scattering.

These 2D images can be converted to a traditional 2-Theta:Theta scan by integrating with respect to chi (tilt) followed by merging data from three frames together. Figure 2 and Figure 4 show the chi-integrated results for the SmartSalt Control and SmartSalt Used acquisitions, respectively. Figure 5 shows an overlay of the data from the Control and Used samples. Note that the Control data, with no collection dust, shows considerable crystalline structure. This structure is also present in the SmartSalt Used data. The SmartSalt Used data also has the relatively small diffraction peaks from the collected dust superimposed on top of the Control-like background. This can make phase identification difficult due to interferences between the Control phases and the phases from the collected dust material.

Figure 6 and Figure 7 show the data from the SmartSalt Control and SmartSalt Used samples, respectively with the selected background and the best matches from the ICDD/ICSD database. The Control sample is composed of polyethylene (PE, high density type) and polypropylene (PP, in two different polymorphs). Also matching the data is a modified type of polyethylene terephthalate. This phase however cannot be positively confirmed since it completely subsides within the PP and PE peaks. There is also very likely to be an amorphous peak within the region of the PP and PE peaks due to non-crystallized

hydrocarbons from the polymers.

The SmartSalt Used sample, in addition to the polymers, consists of Quartz (SiO_2), Calcite, Dolomite, Periclase (MgO), and several more complex mineral/clay materials composed including Magnesium Aluminum Silicates, Sodium Silicates Hydrates, and Aluminum Hydroxides. It is highly likely that there are other clay-type phases present but they could not be identified since their characteristic peaks occur at low 2-Theta angles where there is severe interference from the polymer matrix.

Because the polymer backing/collecting material is so dominant and intense, an attempt was made to subtract the Control background from the Used data to better observe the diffraction peaks from the collected material without the polymer peak interferences. Figure 8 shows the SmartSalt Control (purple trace) and Used (black trace) data superimposed and scaled to match as best as possible in the low angle polymer-dominated region. The dark brown trace is the resultant after subtracting the Control from the SmartSalt Used data. Figure 9 shows the resultant subtracted raw data with a smoothing function applied. Figure 10 is the subtracted data with the selected background and the best matches from the ICDD/ICSD database applied. The same phases appear in the subtracted data as in the standard SmartSalt Used data. However, the subtracted data suggests that the Gibbsite (Aluminum Hydroxide) phase may not be present or certainly much less intense than in the un-subtracted data due to the polymer peak interferences. Several of the other phases also show reduced intensity in the subtracted data, but there is a significant amount of uncertainty associated due to the subtraction of a large number from a slightly larger number with the resultant being a significantly smaller number.

Photo 5 and Photo 6 show the alignment images from the top collection layer (without backing foam) from the SmartSalt Control and SmartSalt Used samples. These samples were setup for XRD in transmission mode. Figure 11 shows the 2-D detector frames from the SmartSalt Control top layer. Note that there are no strong diffraction arcs or spots in these frames. It was hoped that the SmartSalt Used sample top layer would also have only a background contribution like the Control top layer. However, as can be seen in Figure 12, the SmartSalt Used top layer contains low angle peaks nearly identical to the fully assembled SmartSalt Used data. It appears that the process of collecting and measuring the dust with the SmartSalt device causes some of the backing foam to adhere to the top layer collecting material. Subtraction of the Control from the Used data in this case would not provide any additional assistance in identifying the dust phases. An overlay of the SmartSalt Control top material and the SmartSalt Used top material (plus dust) is shown in Figure 13. The phases identified in the Control and Used samples are summarized in Table 1 above.

Figure 14 shows the XRD data taken from the Scotch Brite Control and Used samples with a linear y-axis scaling. Figure 15 shows the same data overlaid with a small vertical offset for clarity but with a y-axis scaling in log(counts) which tends to greatly emphasize smaller, weaker peaks. As can be seen from these 2 figures, the data from the Used and Control

Scotch Brite samples are quite similar. Figure 16 and Figure 17 show the Scotch Brite Control and Used data, respectively, with selected background and best matches from the ICDD/ICSD database. The single most dominant phase is the abrasive material Corundum (aluminum oxide). A minor phase identified as Al nitride is also present. There are some weak unidentified phases present but none which match up with any of the peaks from the dust collection samples. Therefore it seems likely that either no dust particles were entrapped in the Scotch Brite Used sample or diffraction from any entrapped dust particles were obscured by the much stronger Corundum peaks. It is interesting to note that all of the Corundum peak in the Used sample are smaller than in the Control sample. Presumably this is due to loss of the corundum abrasive particles during abrading for dust collection. The changes in some of the smaller, weaker peaks are thought to be due to loss or changes in the (organic?) binder used to adhere the corundum abrasive particles to the Scotch Brite's backbone polymer material. The phases identified in the Scotch Brite samples are summarized in Table 2 above.

Photo 7 and Photo 9 show the low magnification images of the Filter paper Control and Filter paper Used, respectively. Photo 8 and Photo 10 are the respective high magnification alignment images of the Control and Used Filter paper samples. Note that the dark smudge on the Filter paper Used photo is somewhat indistinct and not as dark as the corresponding area on the SmartSalt Used sample. Figure 18 and Figure 19 show the 2-D detector frames acquired for the Filter paper Control and Filter paper Used, respectively. It can be seen immediately that the Filter paper Control has some strong diffraction arcs and is similar (but not identical) to the SmartSalt Control (full assembly) data. The 2-D data from the Filter paper Used in Figure 19 shows some bright spots and weak partial arcs from the dust particles collected on the filter material. But it is quite apparent that the difference between the Control and Used frames is not large and therefore the contributions to the XRD data from the dust particles will not be large.

Figure 20 shows an overlay of the chi-integrated data from the Filter paper Control and Filter paper Used. Again, there is not a large difference between the two scans. Figure 21 and Figure 22 show the data from the Filter paper Control and Used, respectively, with selected background and best matches from the ICDD/ICSD database. The Filter paper Control shows only PET (polyethylene terephthalate) present, but unfortunately, the reference data does not extend to angle greater than 55°. There is some difference between the experimental peak heights and the reference marker heights (proportional to intensity for a perfectly random material) especially around the 42° peak. This may be due to texturing of the PET or possibly another unknown phase. The phases identified in the Filter paper Used include the PET and a number of the same phases as identified in the SmartSalt Used samples. However, not as many phases are identified in the Filter paper Used sample in part due to weaker signals from the dust (i.e. lower dust particle density or dispersion of the dust within the thicker Filter paper Used material). The only phase in the Filter paper Used that was not found in the SmartSalt samples is an iron oxide, Magnetite. However, since the dust particles in the Filter paper Used were acquired by abrading the canister with the Scotch Brite, some abrasion of the stainless steel (or other steel), the observation of Fe oxide particles would be expected. The phases identified in the Filter paper Control and Used samples are summarized in Table 3 above.

After reviewing this report, you may assess our services using an electronic service evaluation form. This can be done by clicking on the link below, or by pasting it into your internet browser. Your comments and suggestions allow us to determine how to better serve you in the future.
http://www.eaglabs.com/main-survey.html?job=C0DHY160

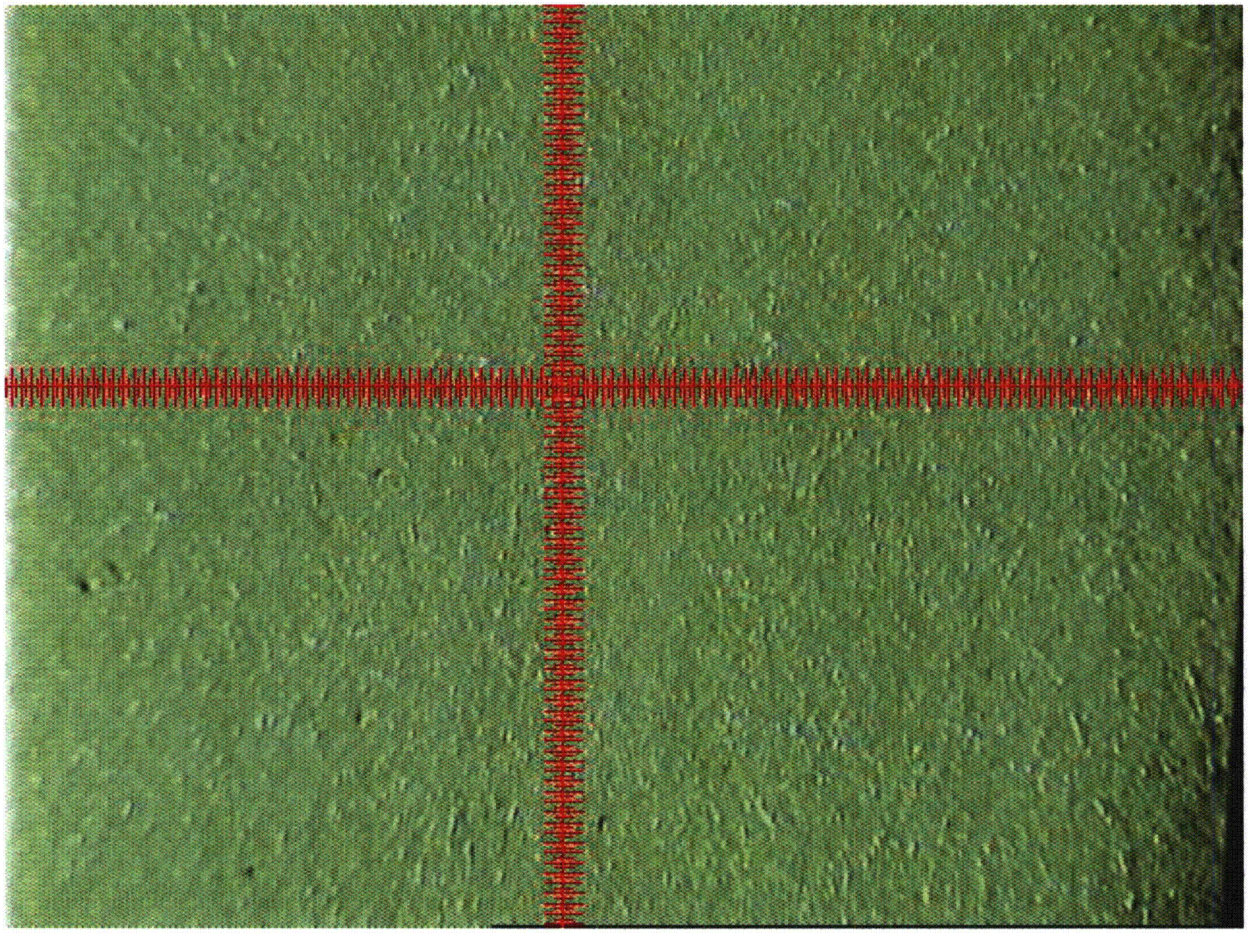

Photo 1: Low magnification image of

SaltSmart Control

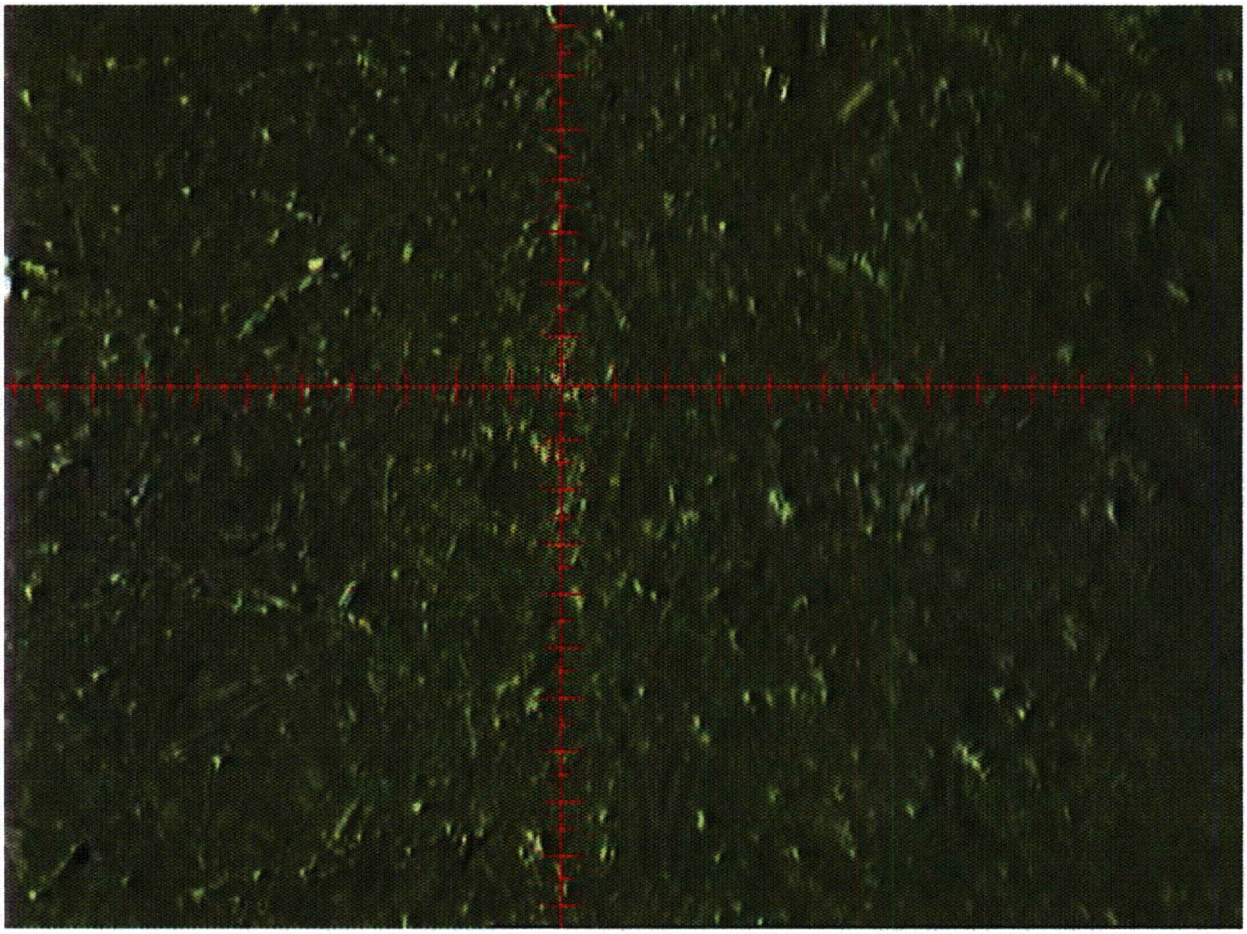

Photo 2: High magnification alignment image of SaltSmart Control

(Laser alignment spot barely visible. Large tic spacing = 100µm.)

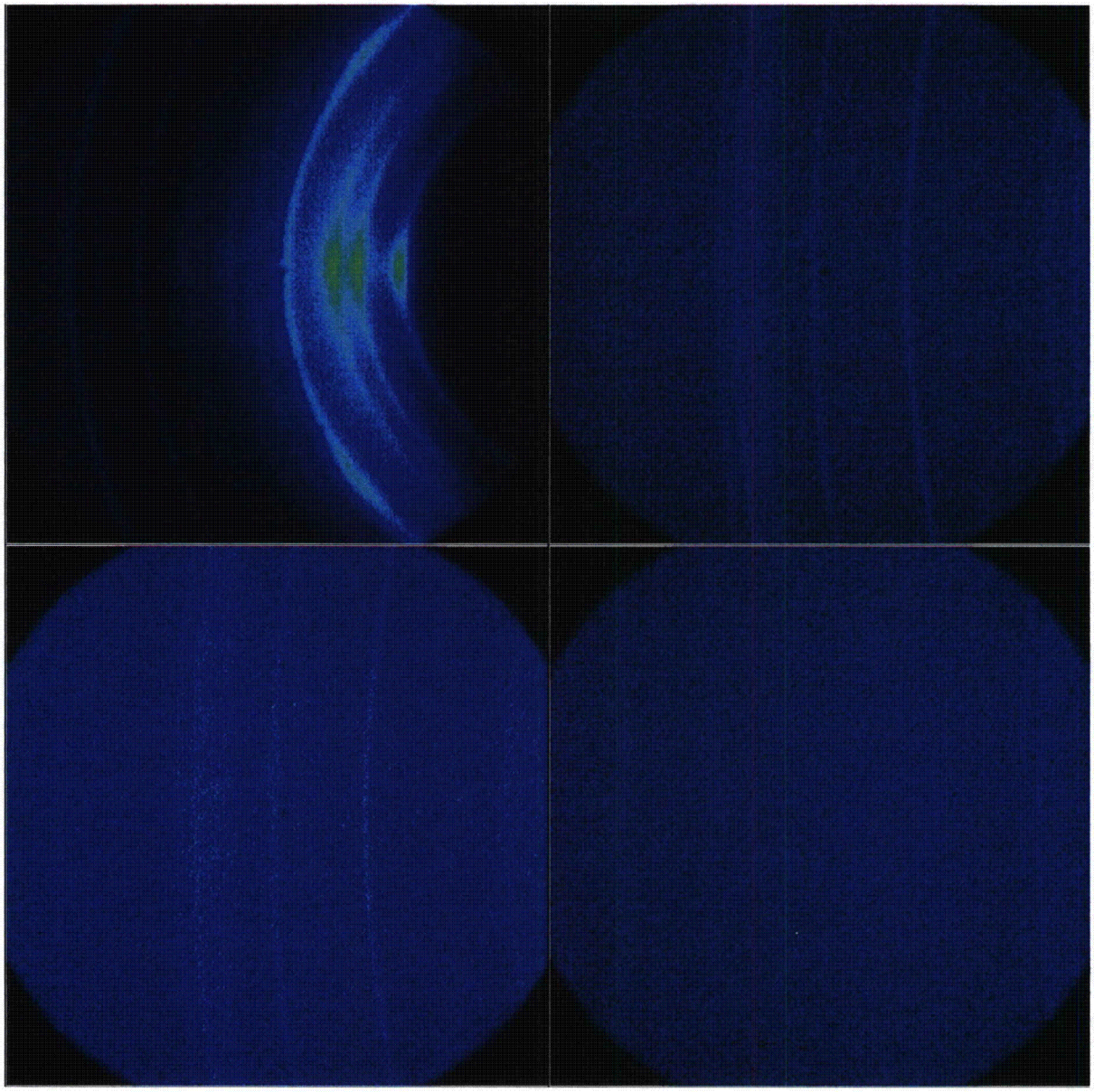

**Figure 1: 2-D detector frames acquired at 2-Theta values of 22°, 42°, 62°, and 82°. In each frame, 2-Theta increases from right to left.
Frames shown are for the SmartSalt Control (full assembly).**

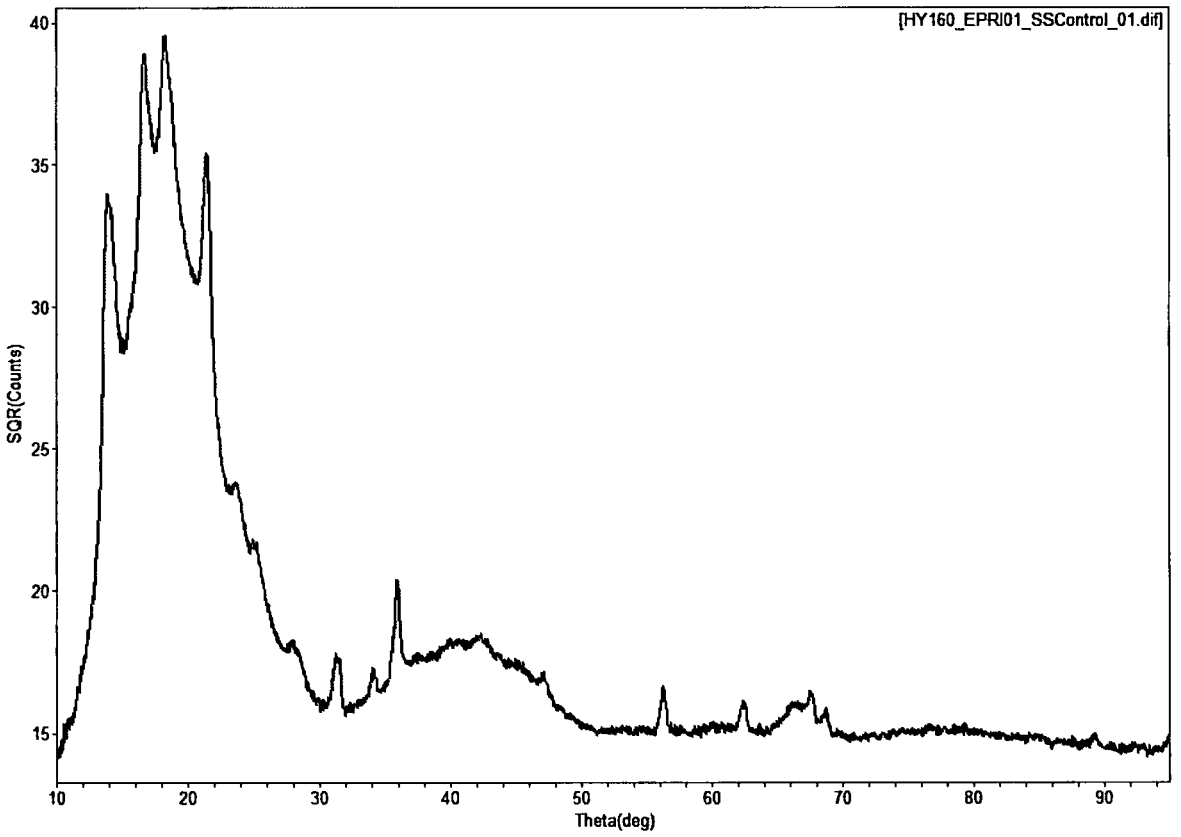

Figure 2: Chi-integrated raw data for SmartSalt Control sample.

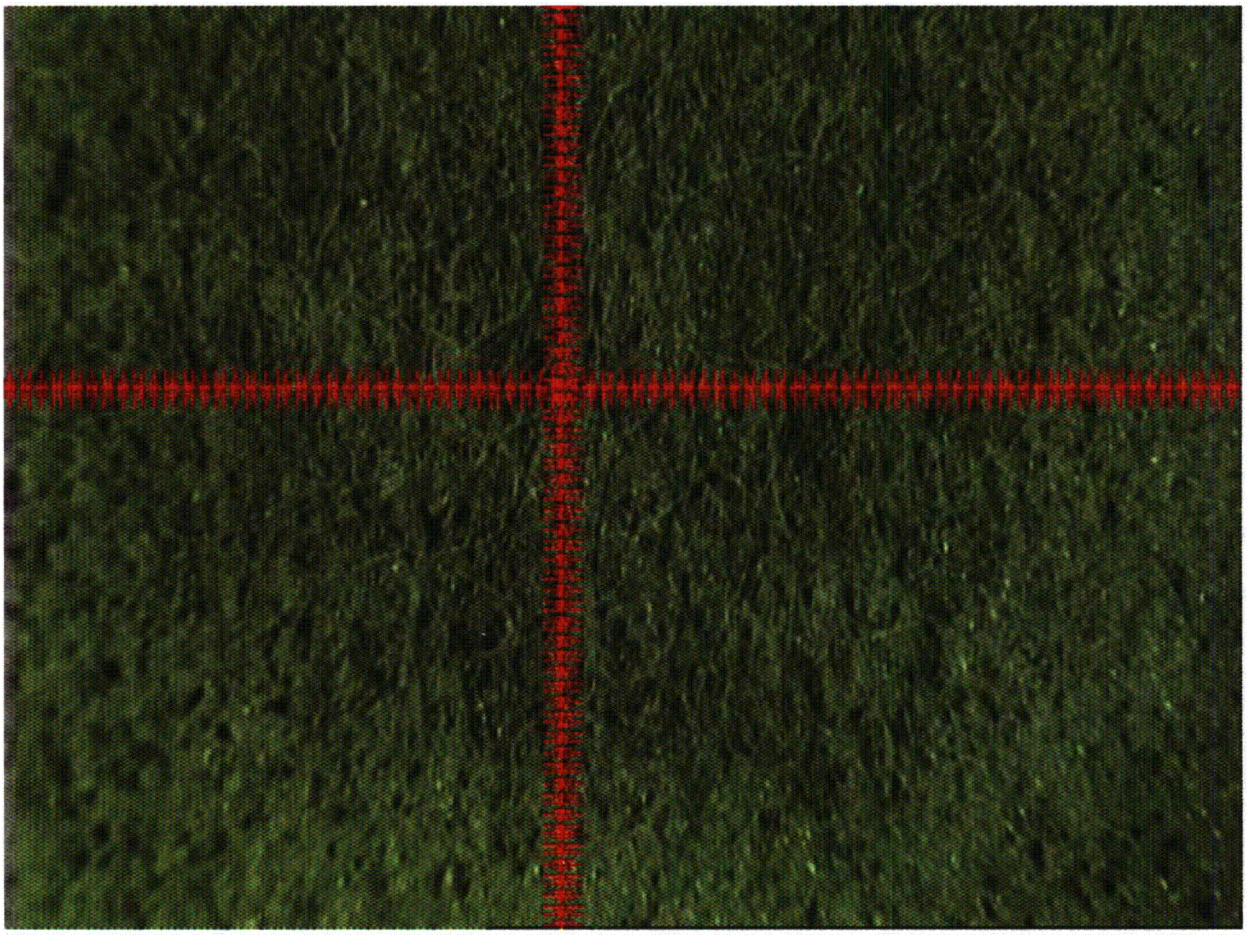

Photo 3: Low magnification image of

SaltSmart Used

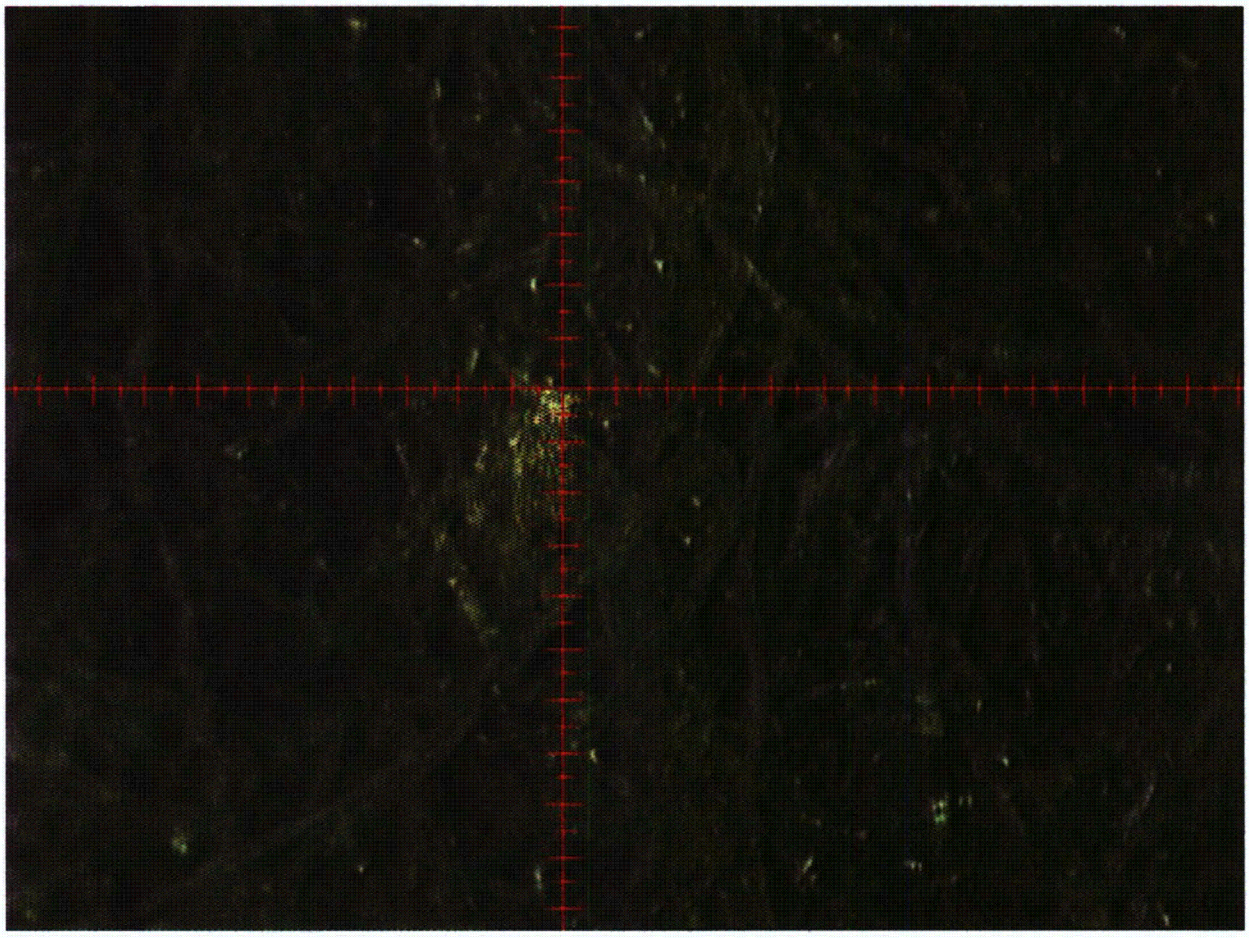

Photo 4: High magnification alignment image of SaltSmart Used

(Laser alignment spot visible. Large tic spacing = 100µm.)

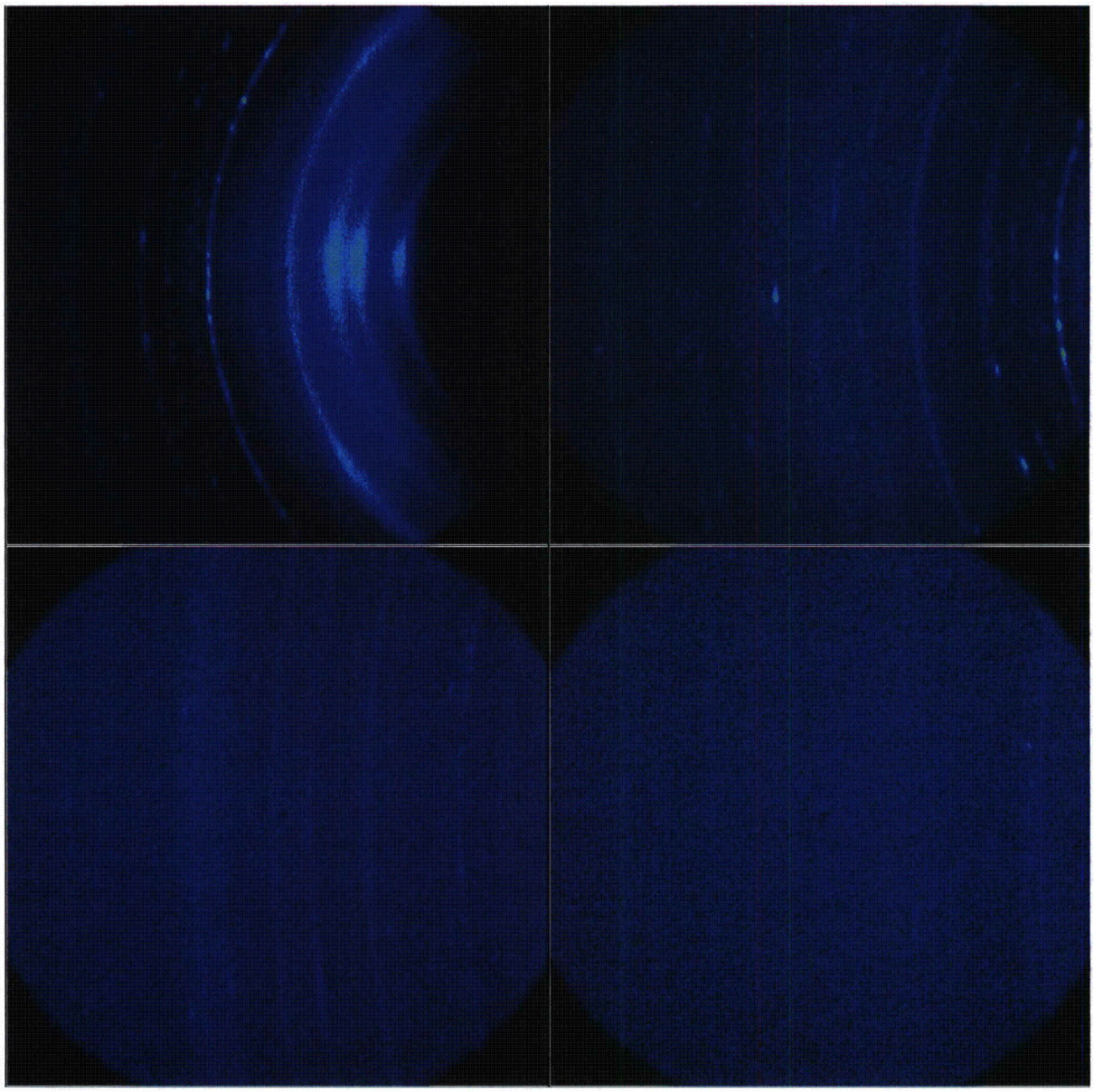

**Figure 3: 2-D detector frames acquired at 2-Theta values of 22°, 42°, 62°, and 82°. In each frame, 2-Theta increases from right to left.
Frames shown are for the SmartSalt Used (full assembly).**

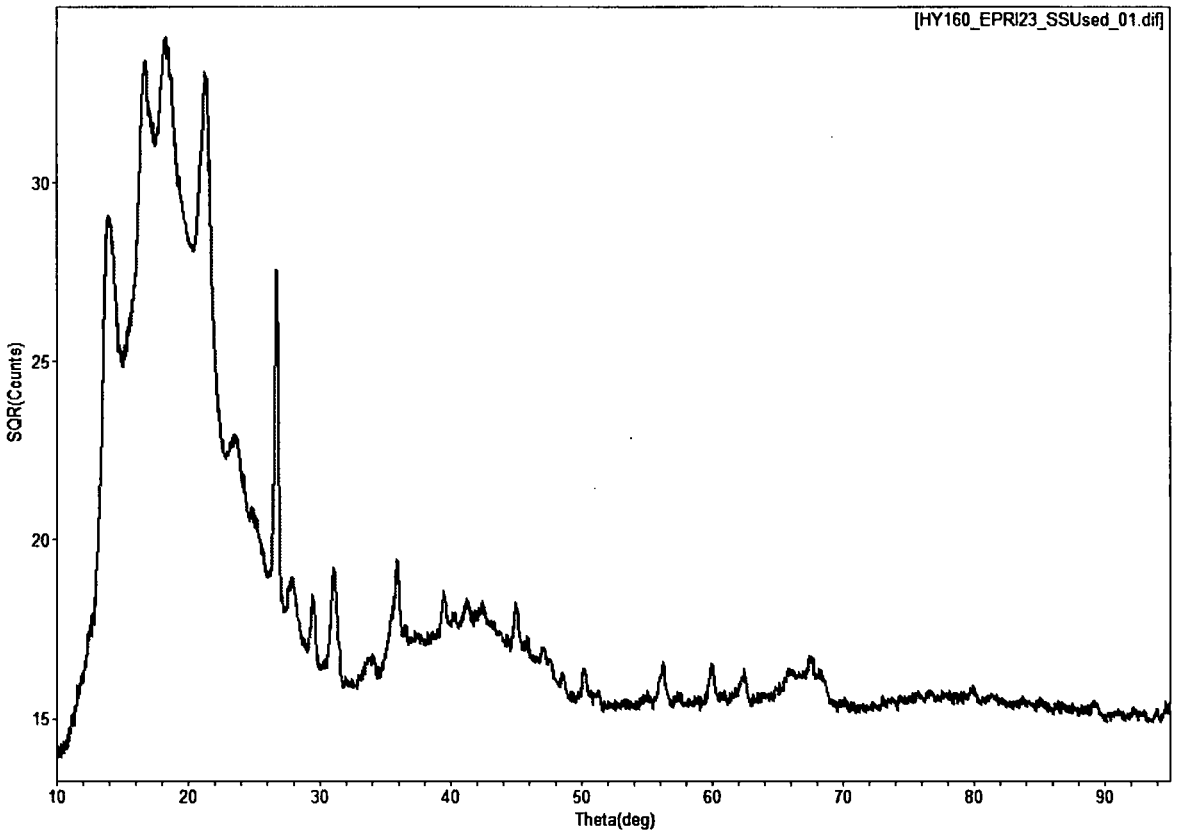

Figure 4: Chi-integrated raw data for SmartSalt Used sample.

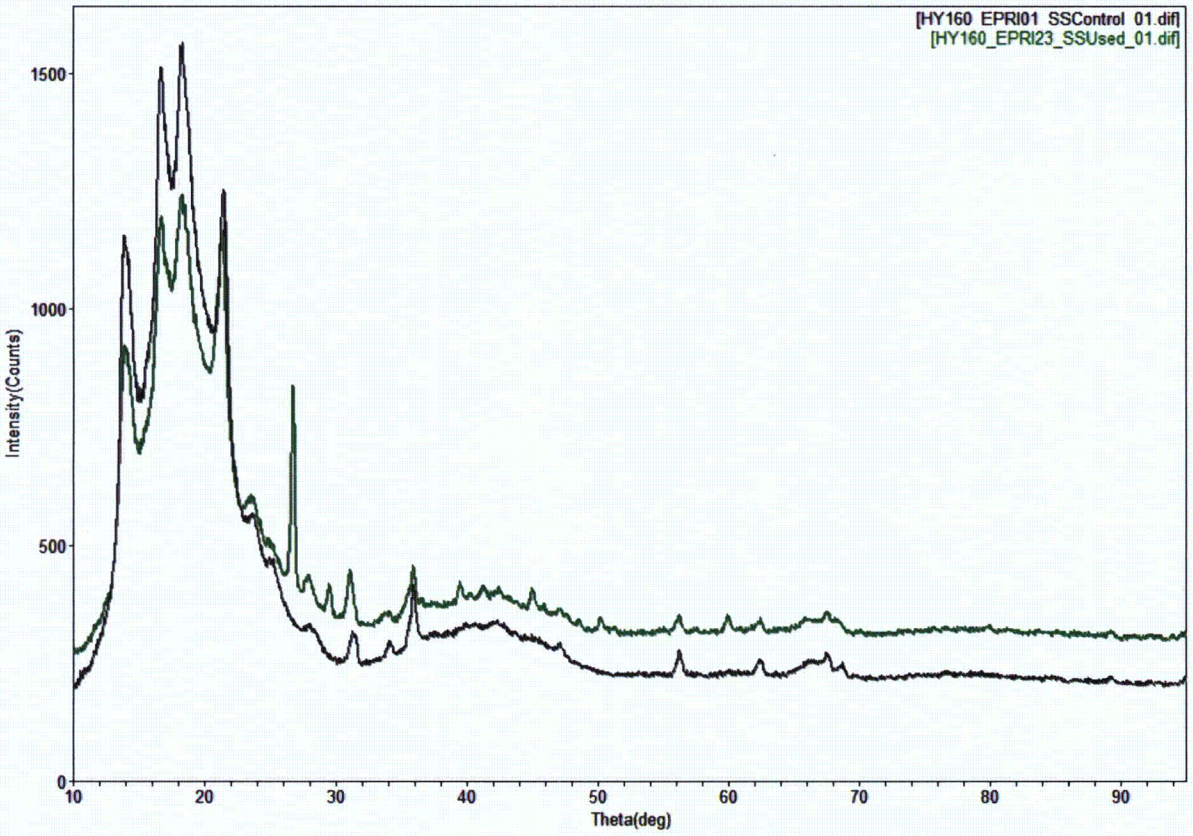

Figure 5: Overlay of XRD data from SmartSalt Control (black) and SmartSalt Used (green).

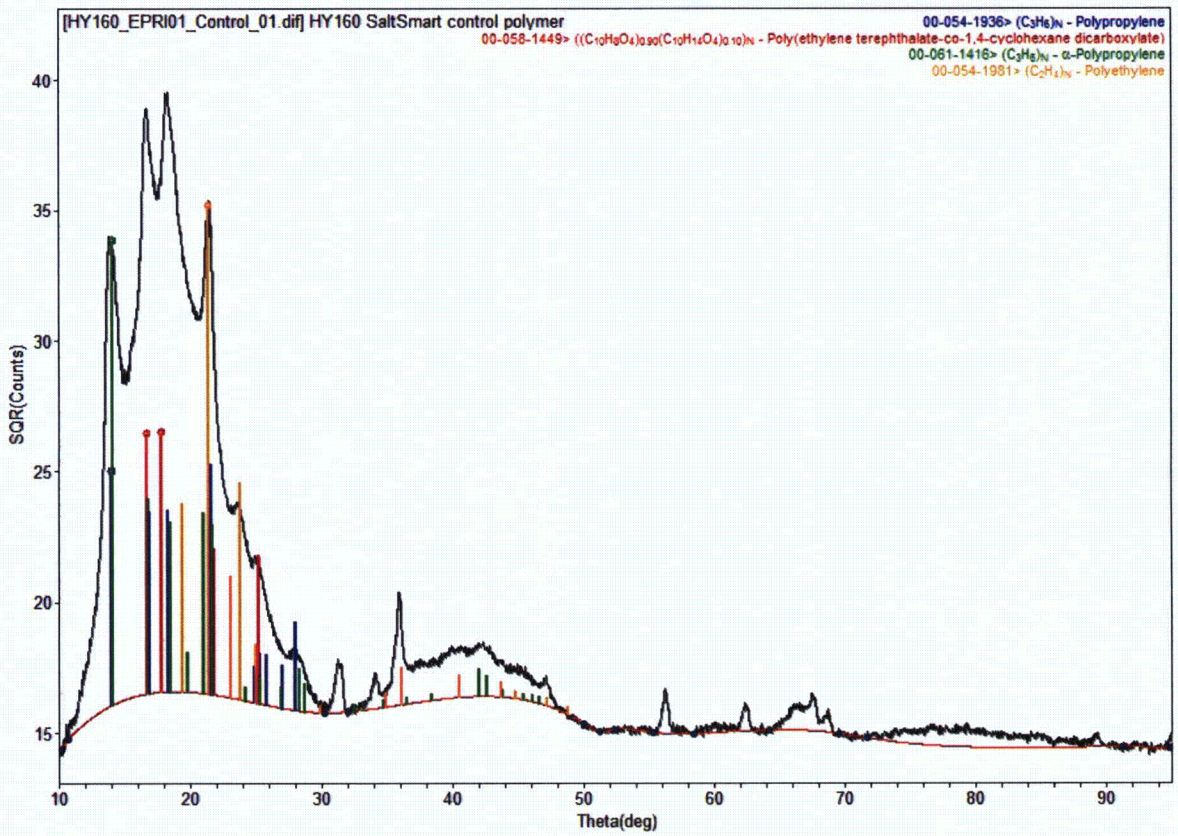

Figure 6: Phase identification of SmartSalt Control sample.

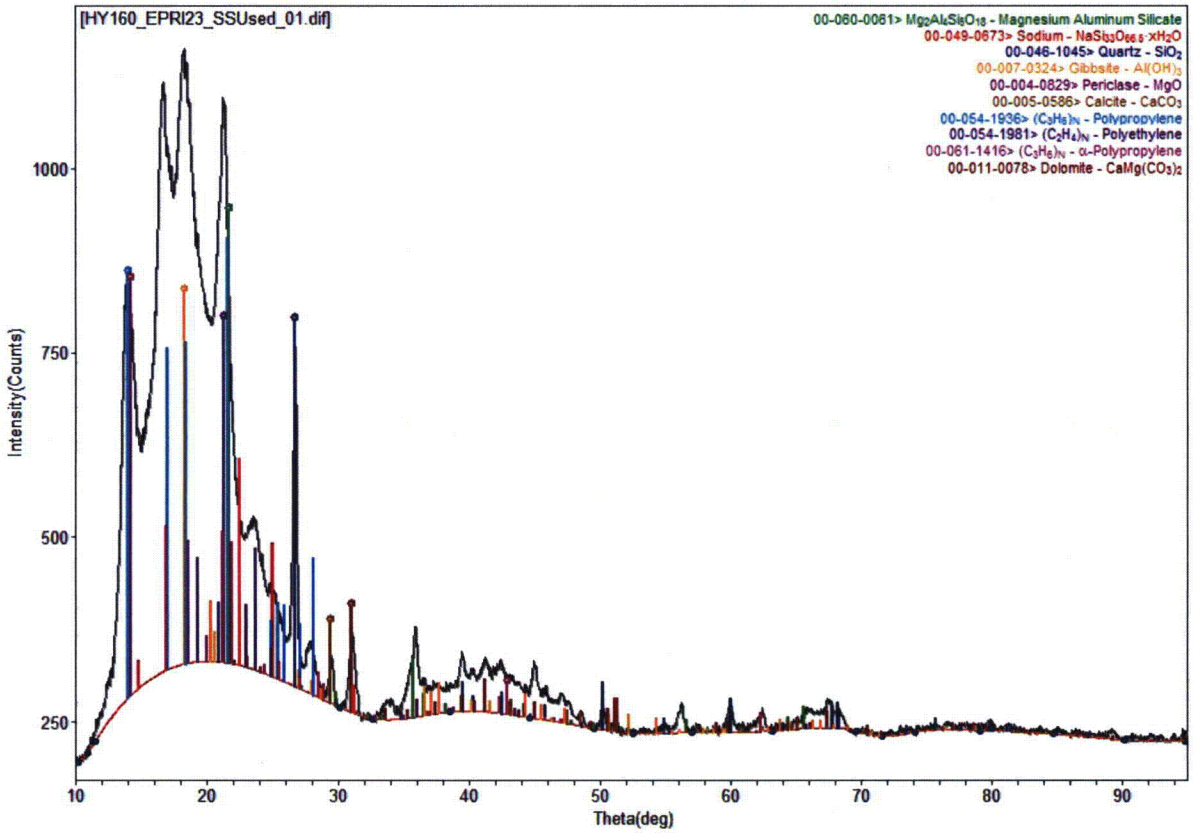

Figure 7: Phase identification of SmartSalt Used sample.

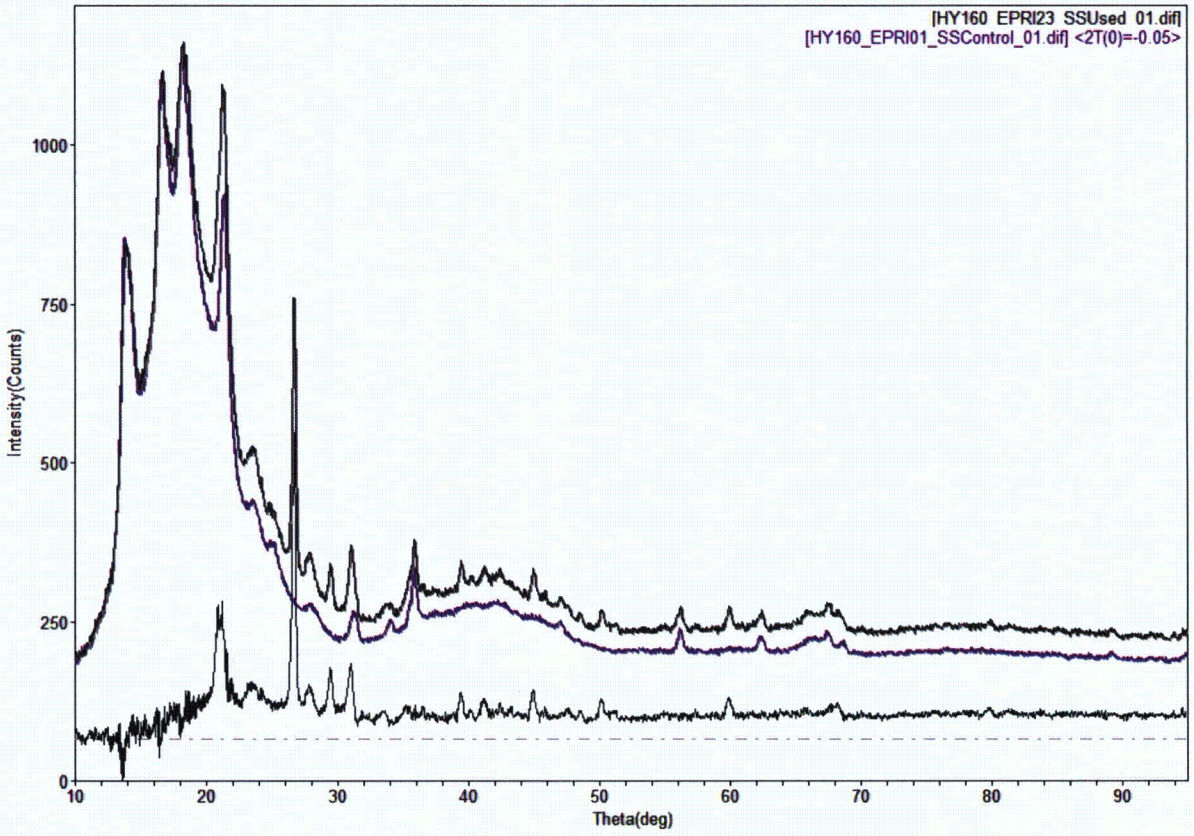

Figure 8: Overlay of scaled and shifted XRD data from SmartSalt Control (purple) and SmartSalt Used (black). The resulting data after subtraction of SmartSalt Control (purple) and SmartSalt Used (black) is show as the lower dark brown trace.

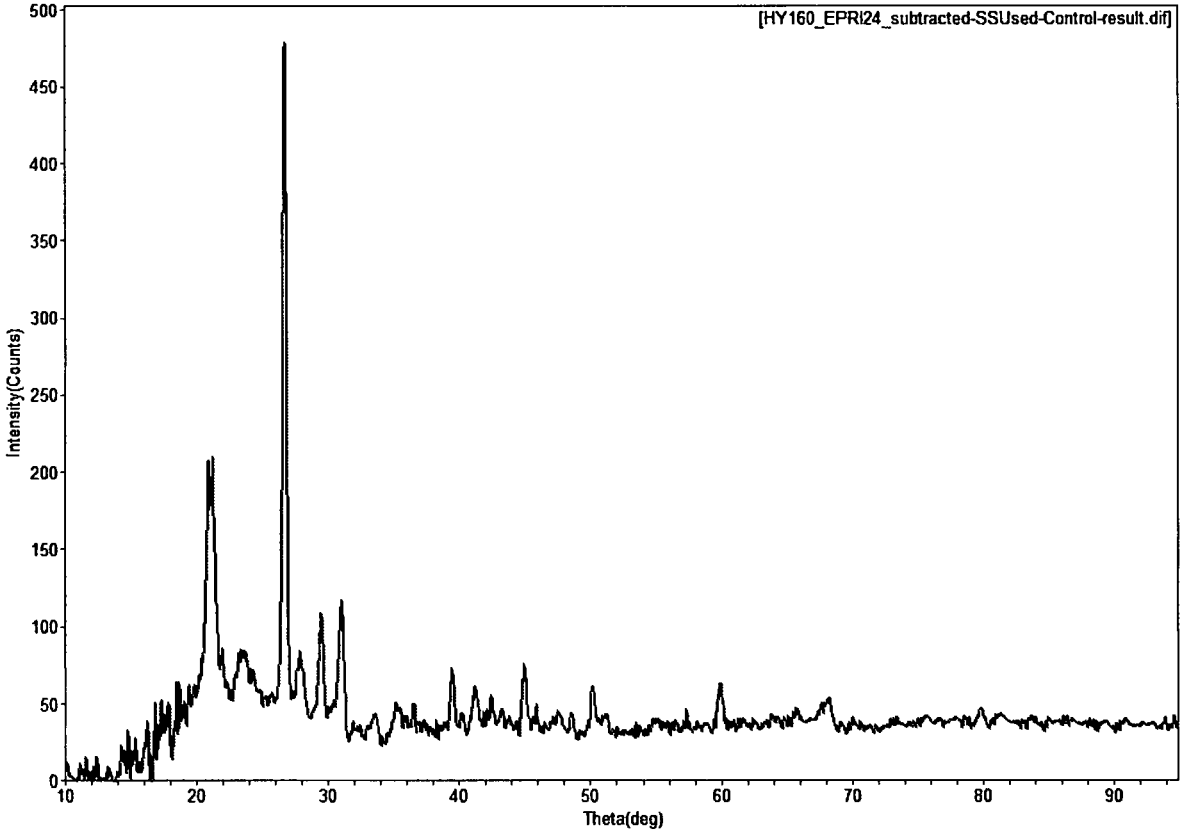

Figure 9: Smoothed resultant scan from subtraction of SmartSalt Control from SmartSalt Used data.

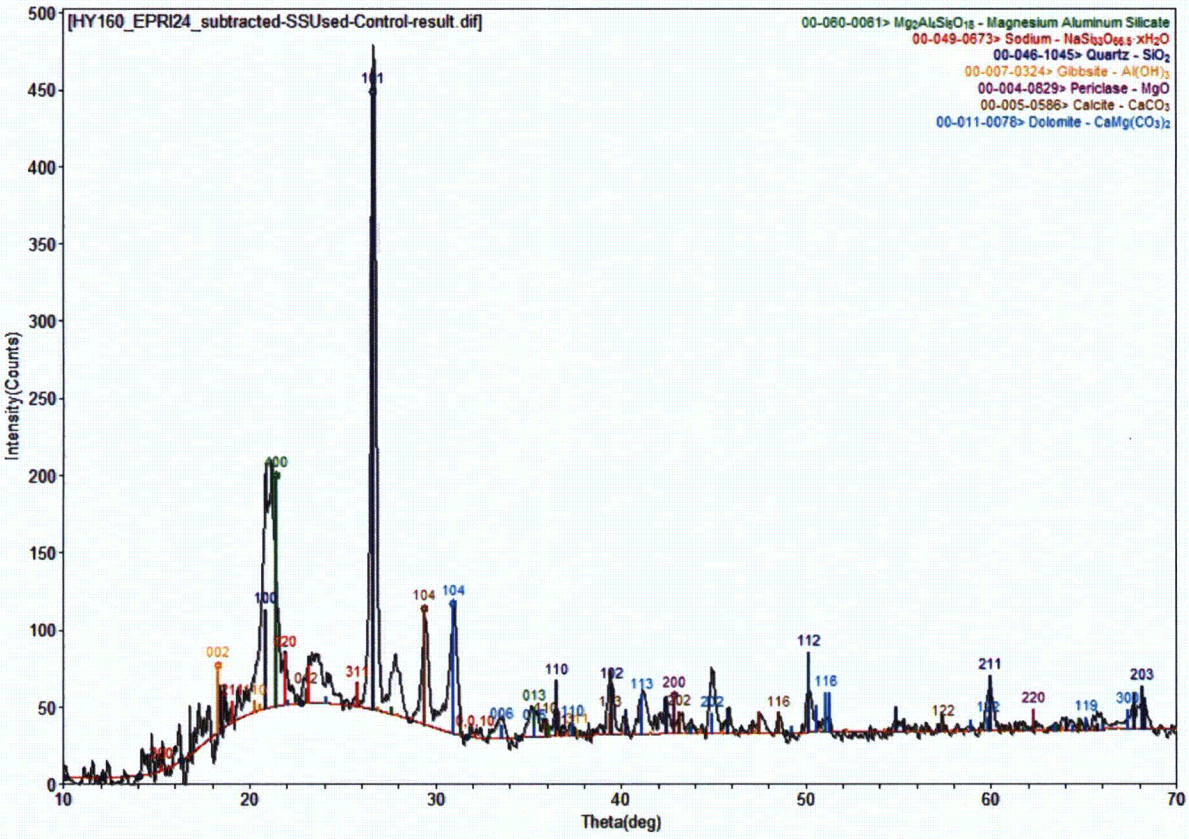

Figure 10: Phase identification of resultant SmartSalt Used minus Control data.

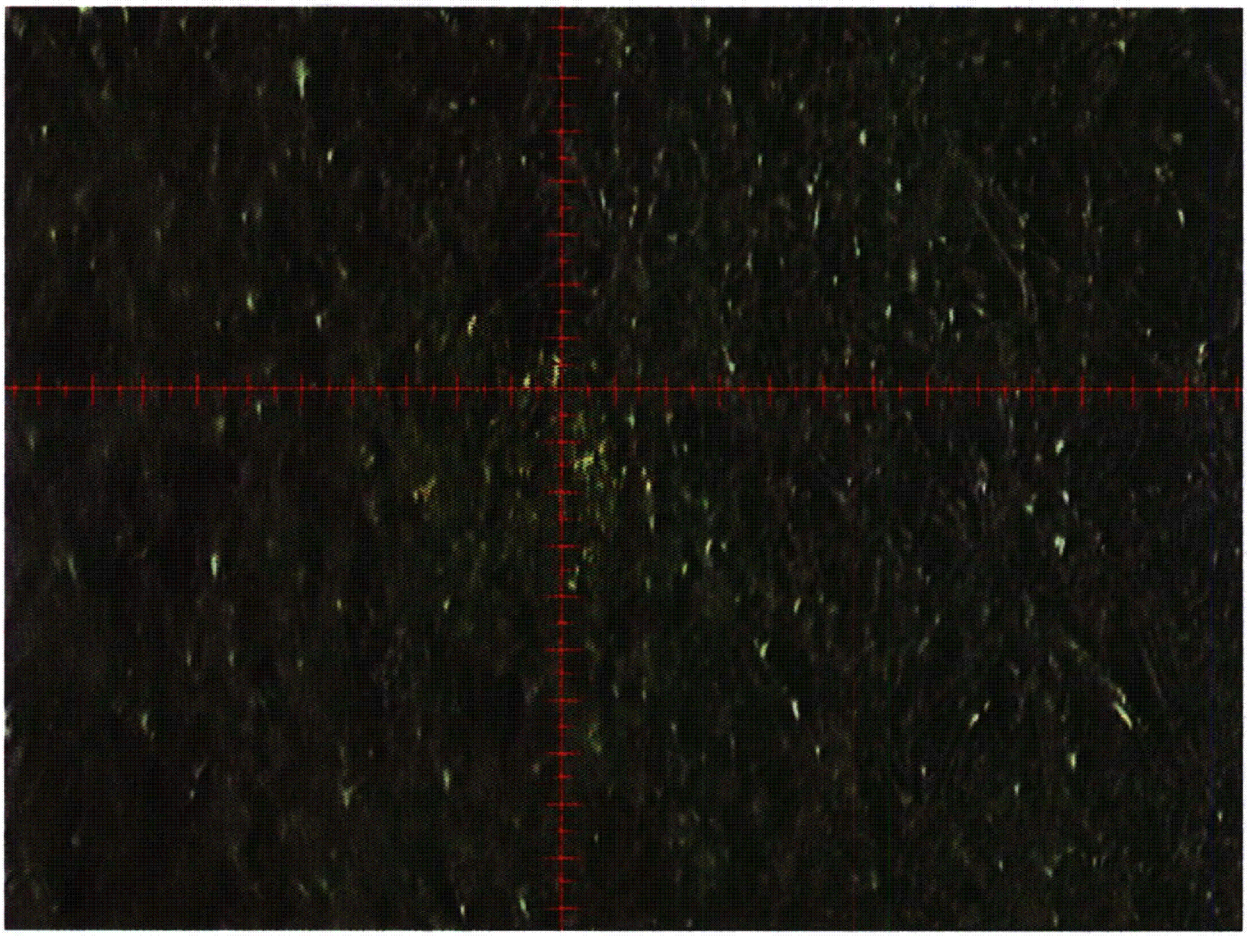

Photo 5: High magnification alignment image of SaltSmart Control top film for transmission XRD

(Laser alignment spot visible. Large tic spacing = 100µm.)

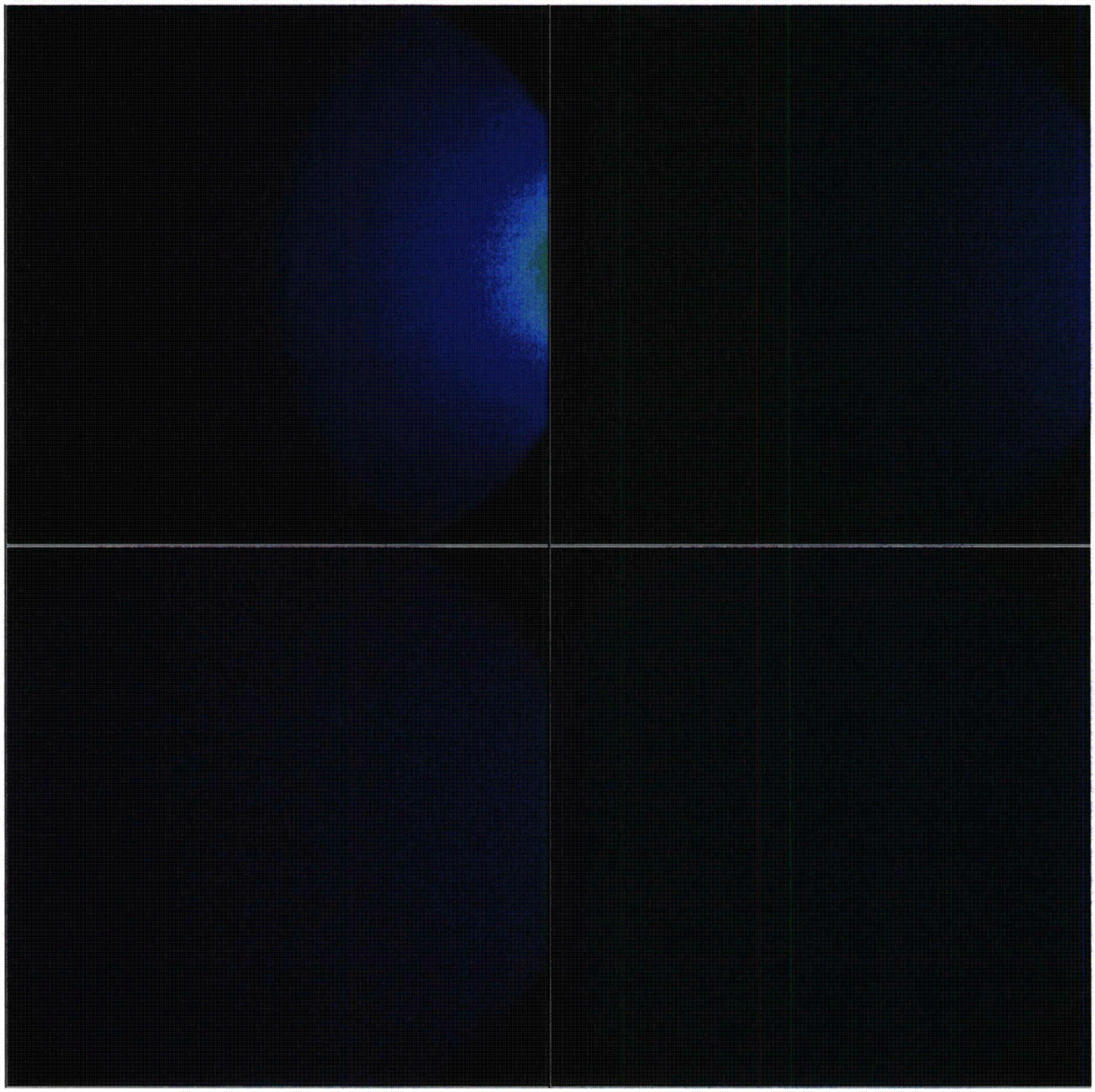

Figure 11: 2-D detector frames acquired at 2-Theta values of 22°, 42°, 62°, and 82°. In each frame, 2-Theta increases from right to left.
Frames shown are for the SmartSalt Control top material (w/o backing)

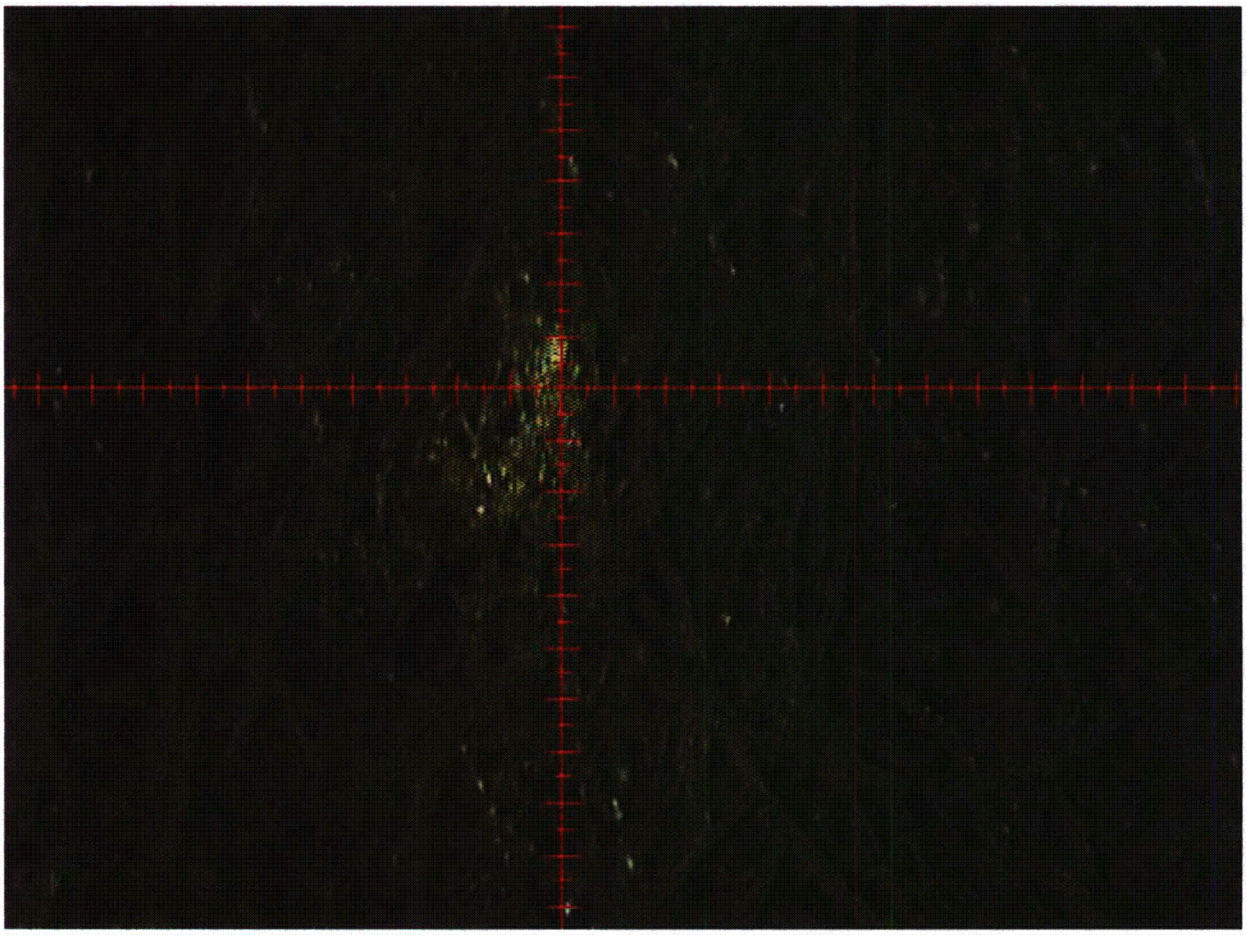

Photo 6: High magnification alignment image of SaltSmart Used top film for transmission XRD

(Laser alignment spot visible. Large tic spacing = 100µm.)

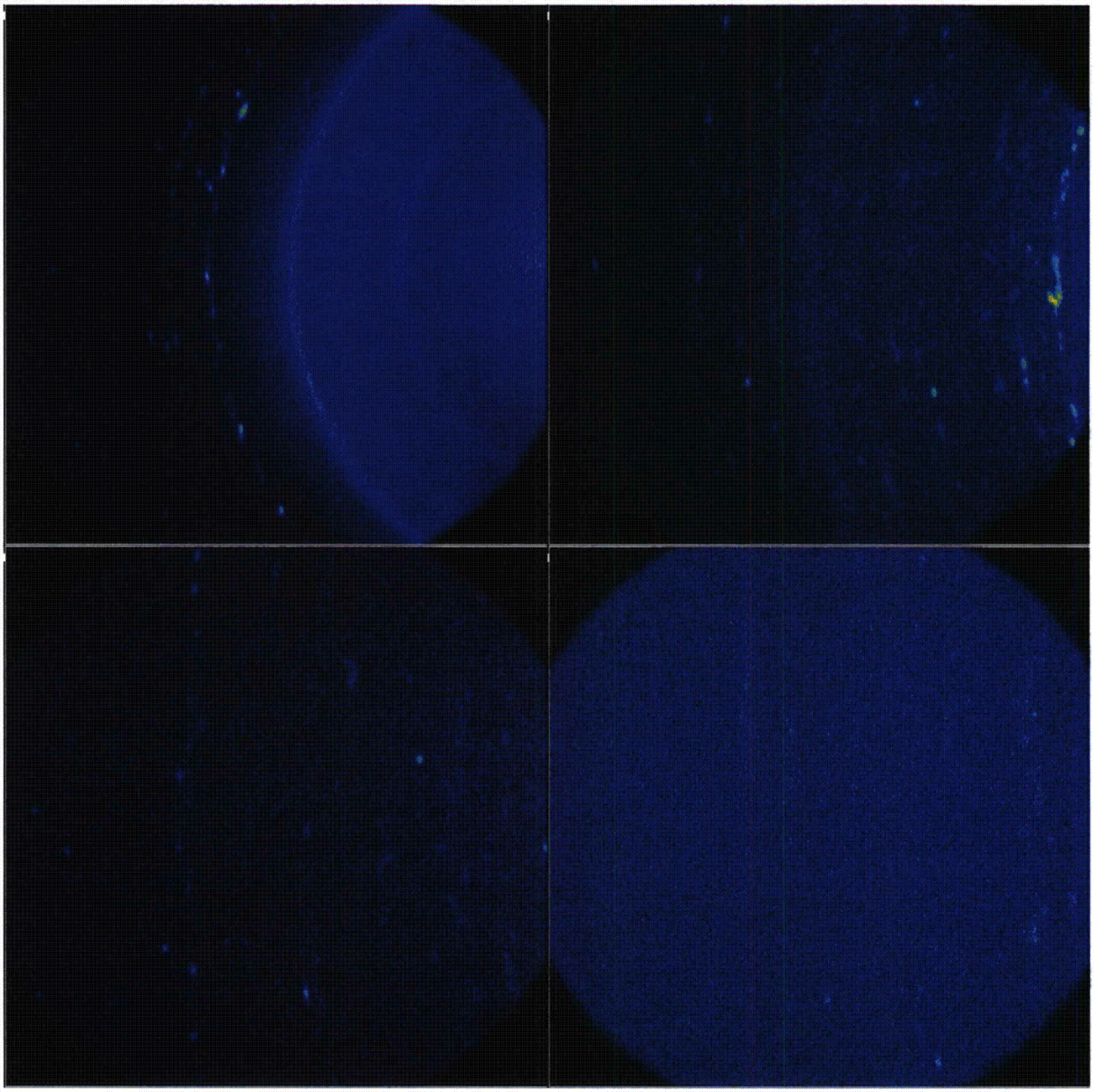

Figure 12: 2-D detector frames acquired at 2-Theta values of 22°, 42°, 62°, and 82°. In each frame, 2-Theta increases from right to left.
Frames shown are for the SaltSmart Used top material plus dust (w/o backing)

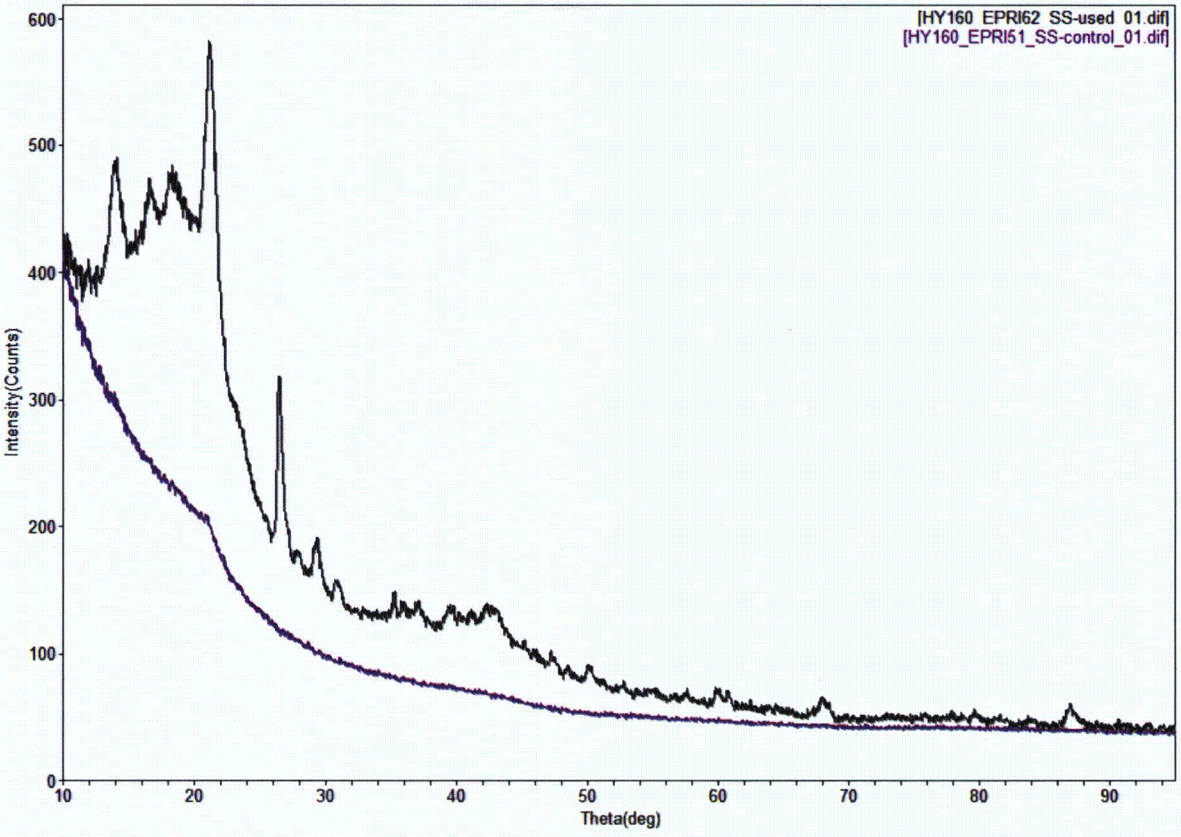

Figure 13: Overlay of data from SmartSalt Control (purple) and Used (black) top material.

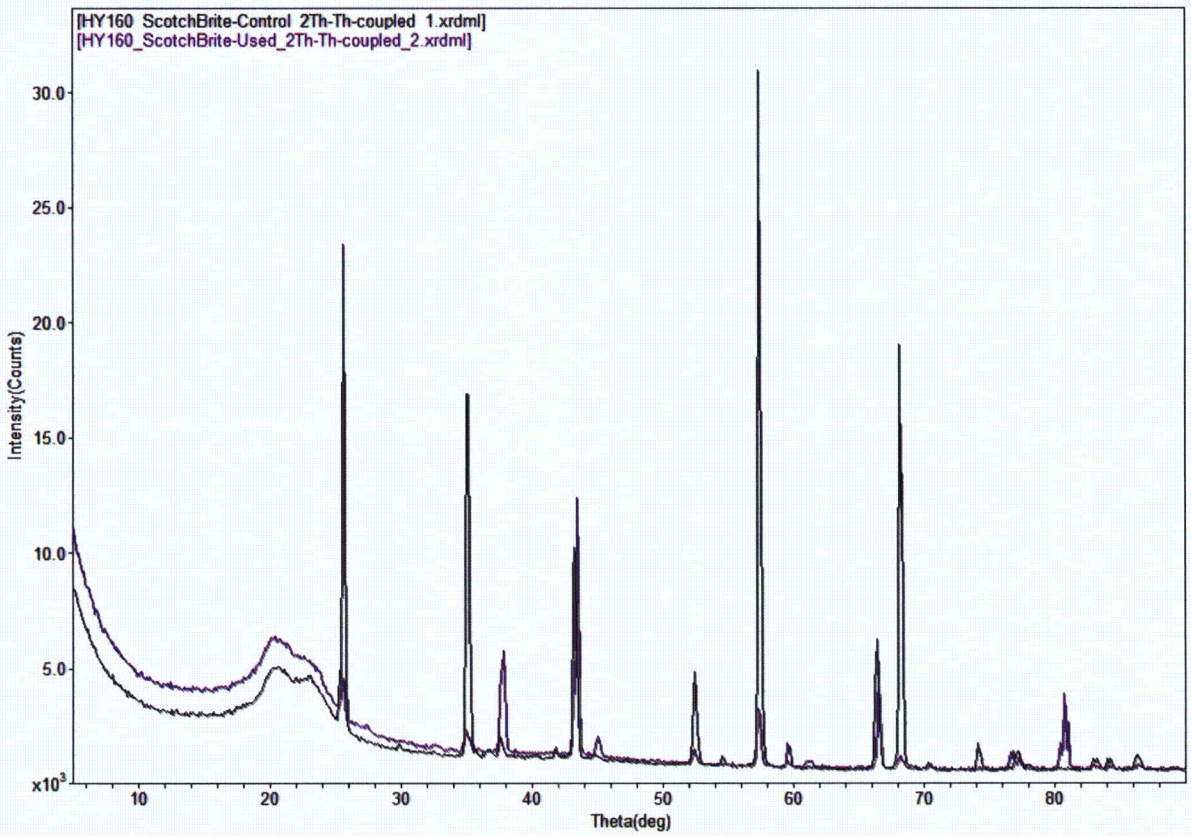

Figure 14: Overlay of data from Scotch Brite Control (black) and Used (purple) samples.

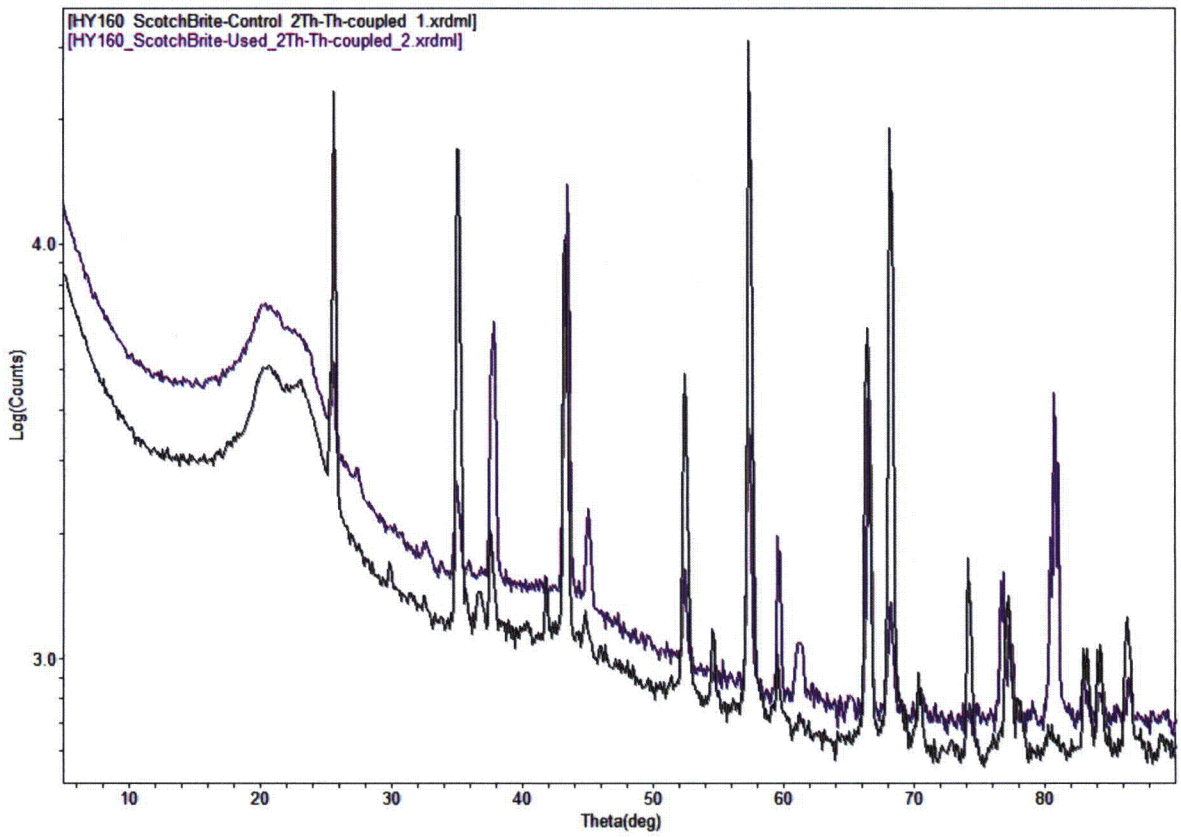

Figure 15: Overlay of data from Scotch Brite Control (black) and Used (purple) samples but with log(counts) scaling and vertical offset applied.

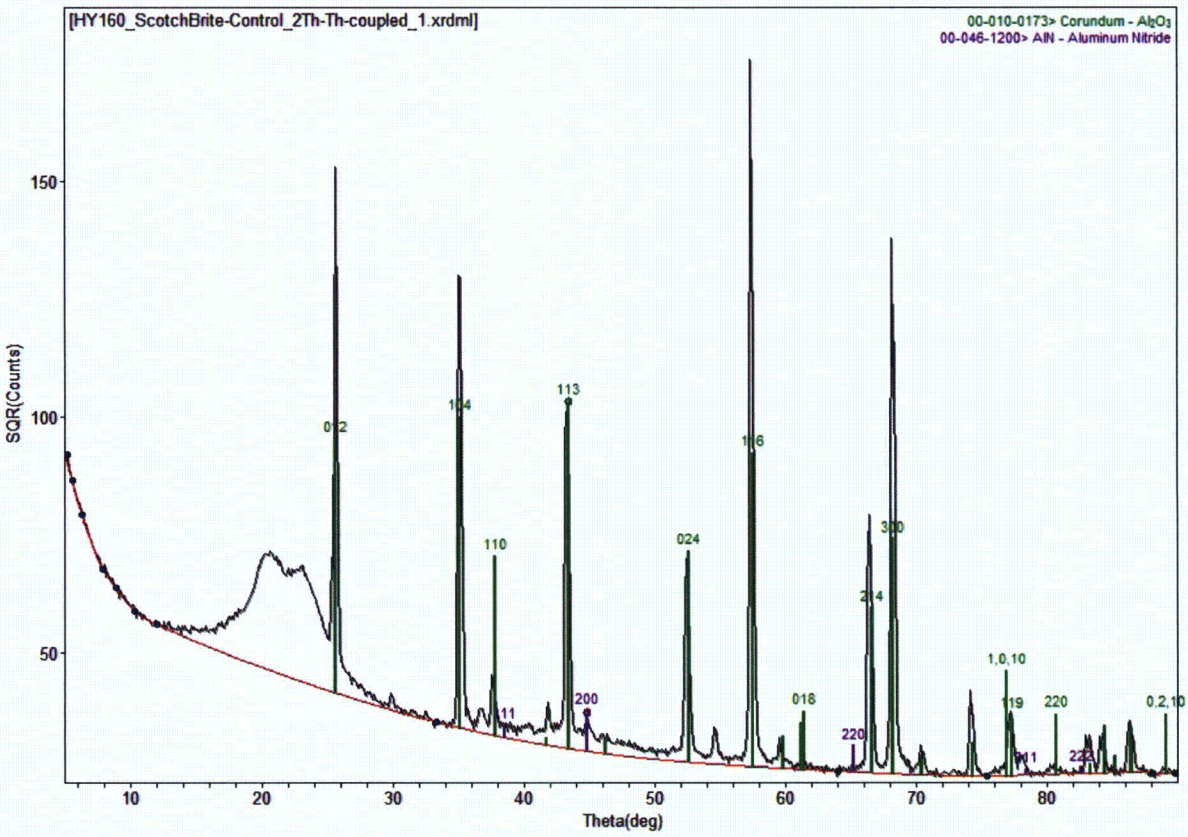

Figure 16: Phase identification of Scotch Brite Control sample.

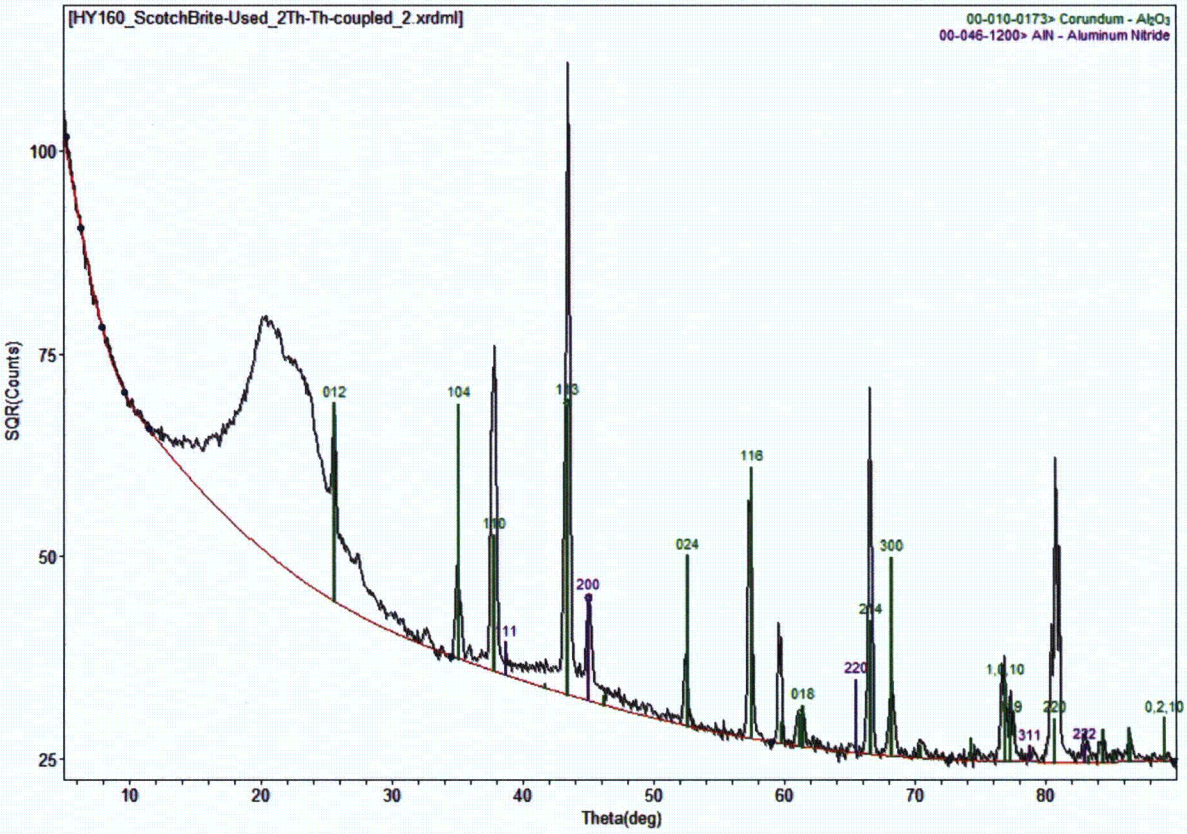

Figure 17: Phase identification of Scotch Brite Used sample.

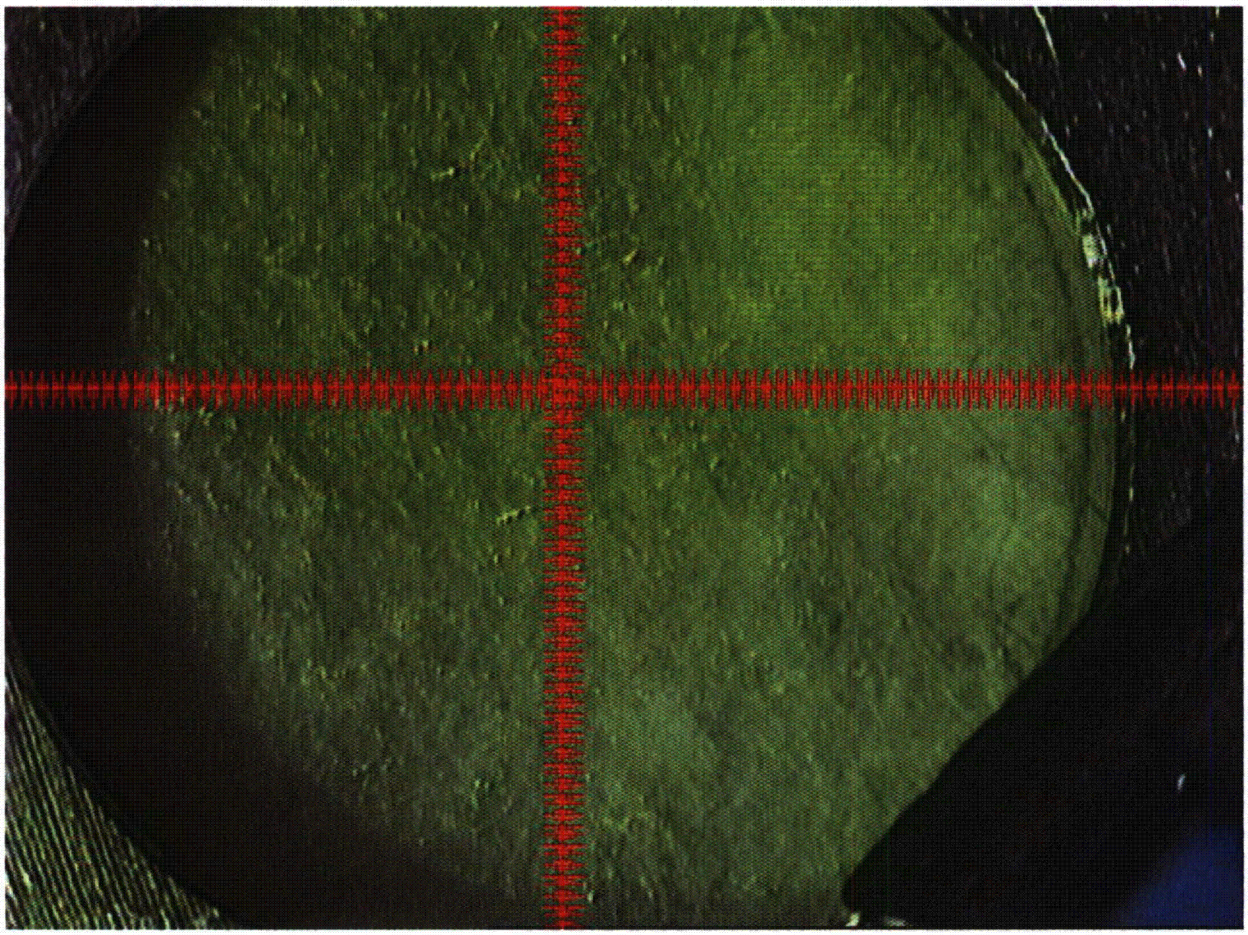

Photo 7: Low magnification image of Filter paper- Control

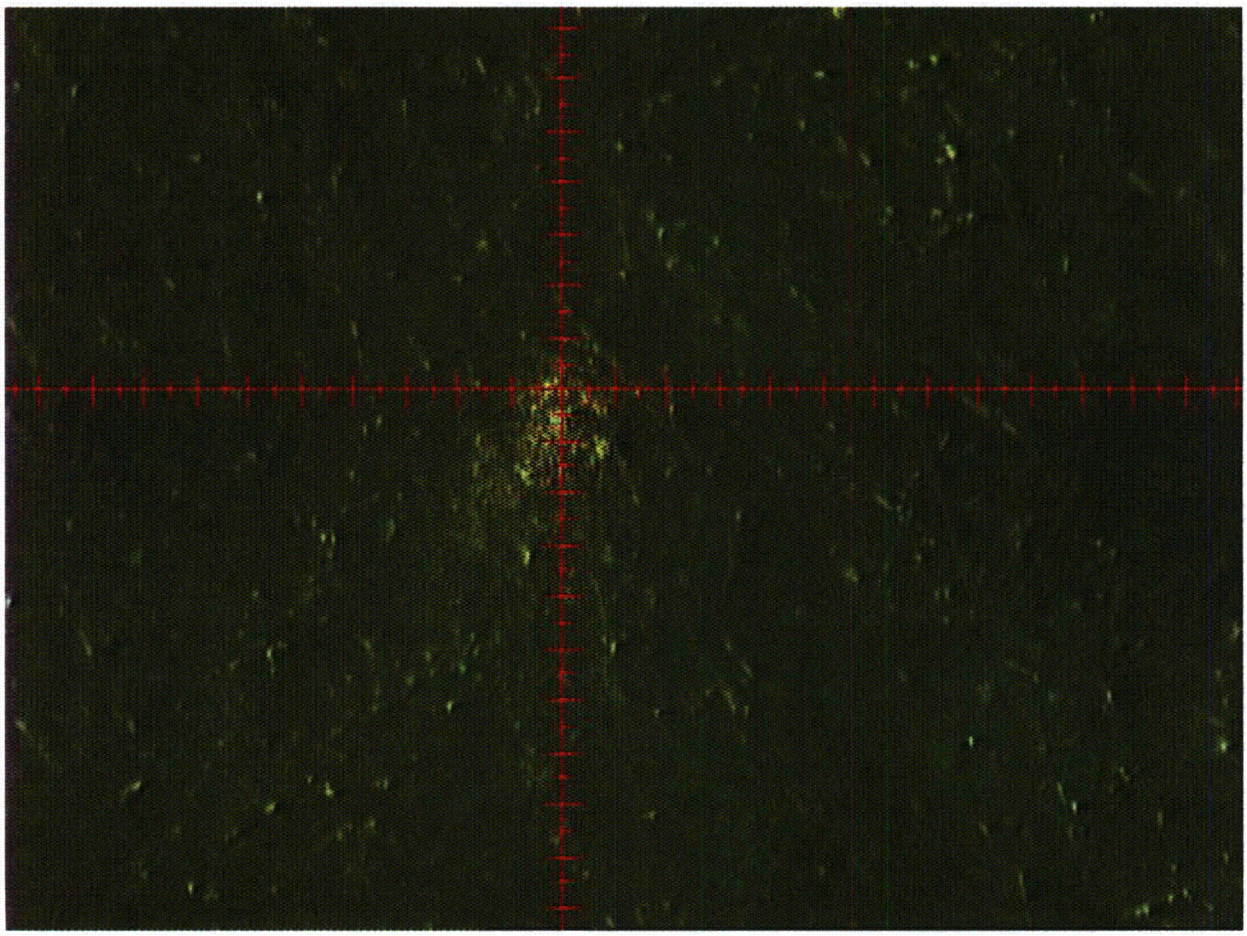

Photo 8: High magnification alignment image of Filter paper- Control

(Laser alignment spot visible. Large tic spacing = 100µm.)

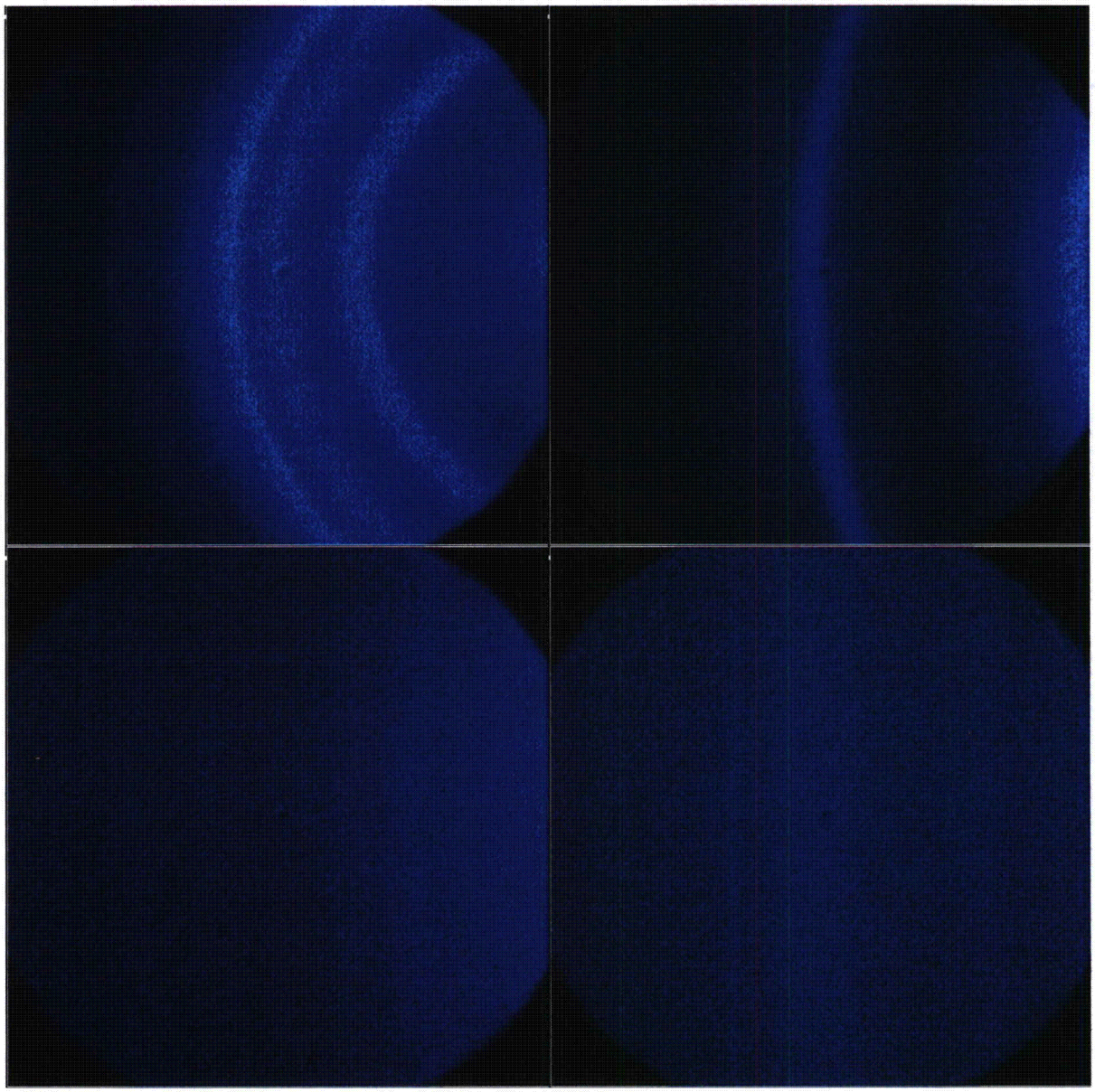

Figure 18: 2-D detector frames acquired at 2-Theta values of 22°, 42°, 62°, and 82°. In each frame, 2-Theta increases from right to left. Frames shown are for the Filter paper Control

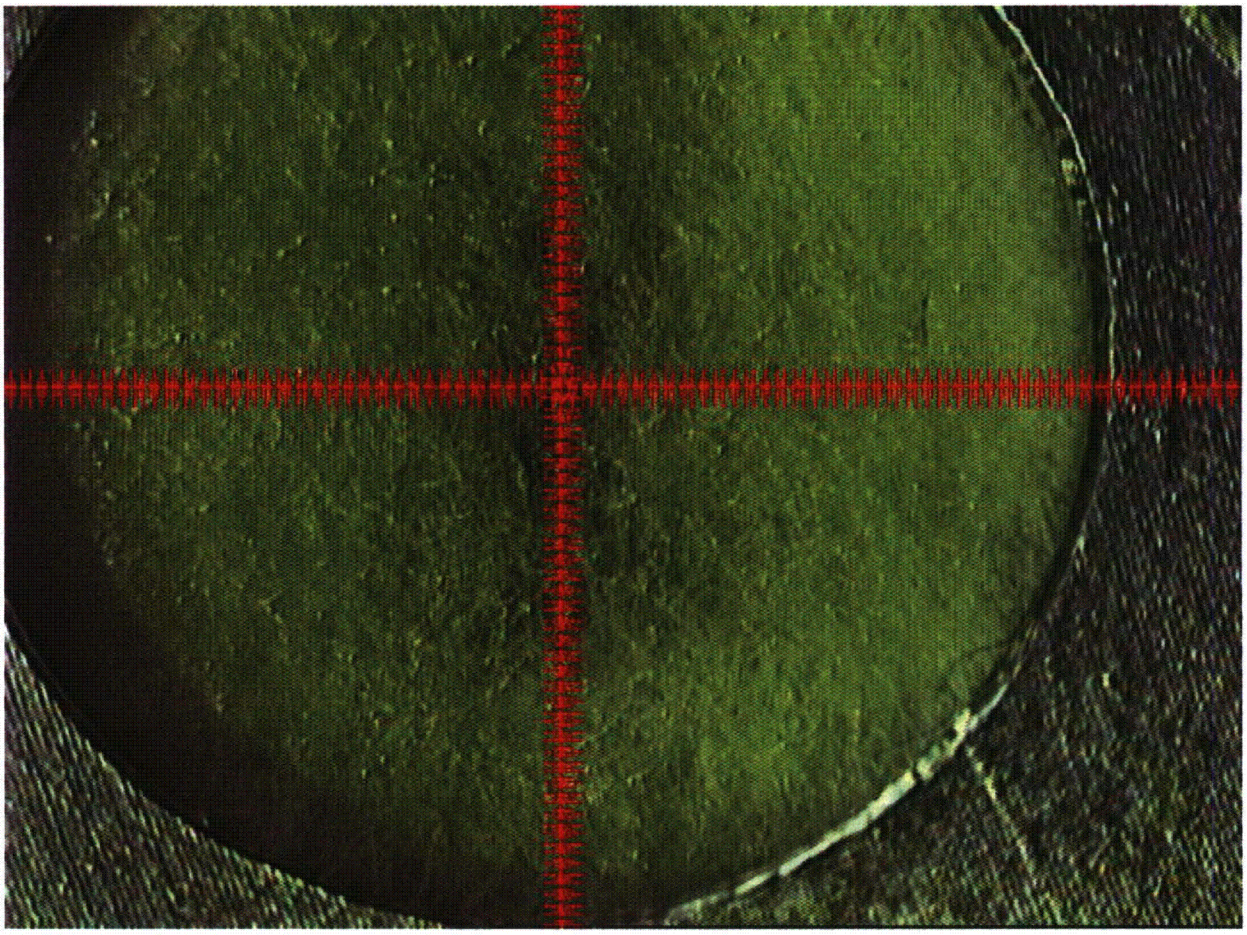

Photo 9: Low magnification image of Filter paper- Used

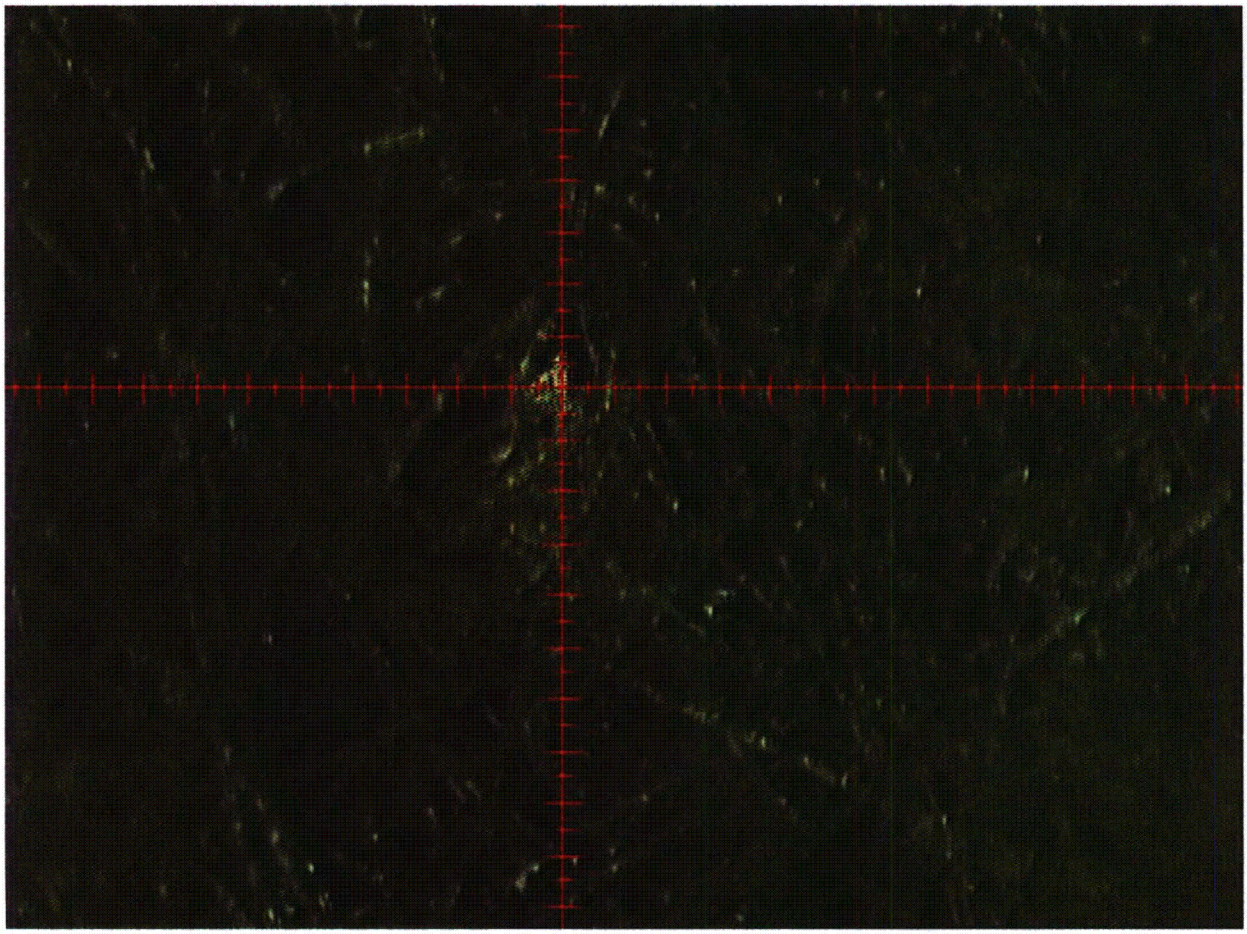

Photo 10: High magnification alignment image of Filter paper- Used

(Laser alignment spot visible. Large tic spacing = 100µm.)

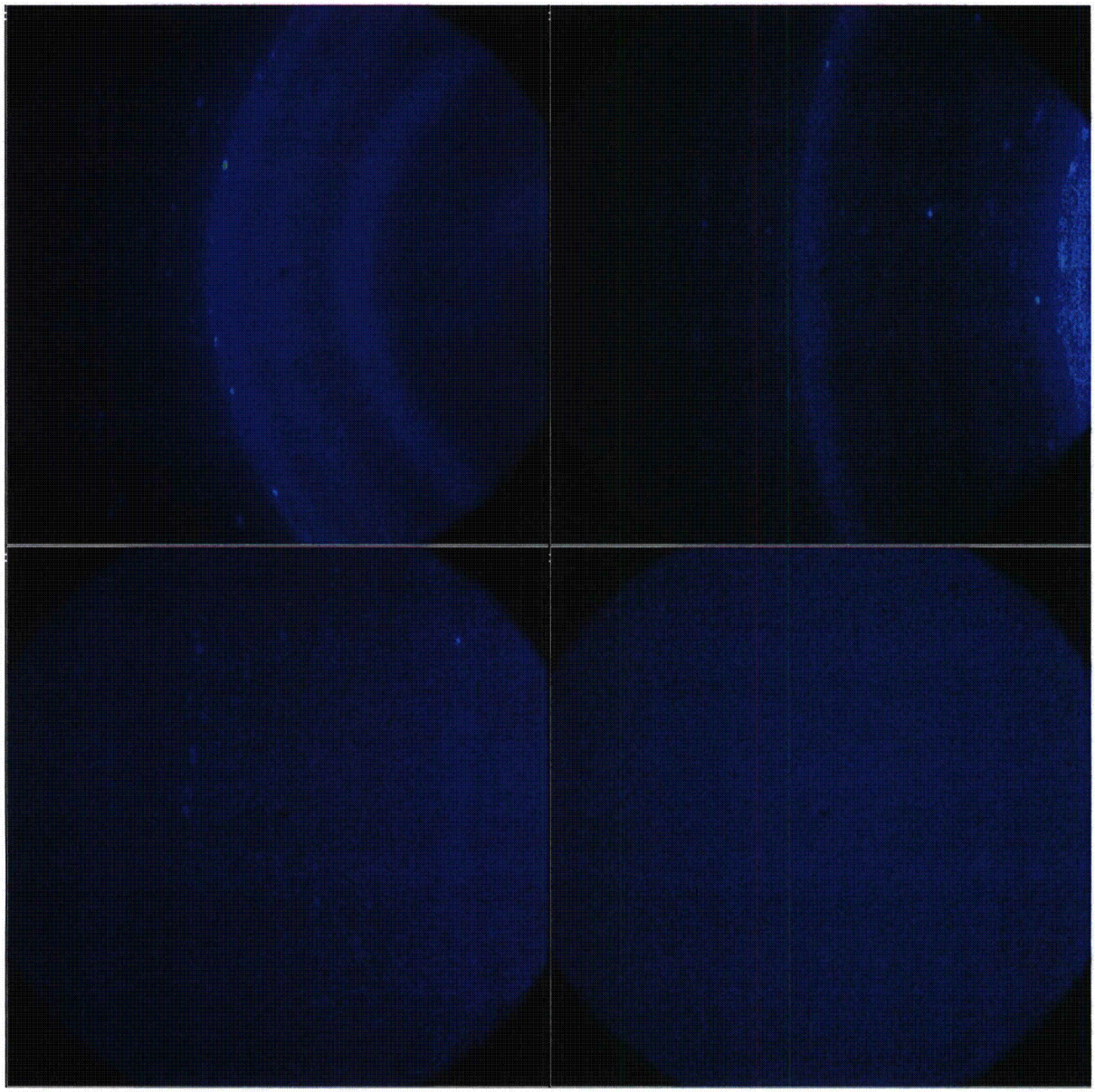

**Figure 19: 2-D detector frames acquired at 2-Theta values of 22°, 42°, 62°, and 82°. In each frame, 2-Theta increases from right to left.
Frames shown are for the Filter paper Used**

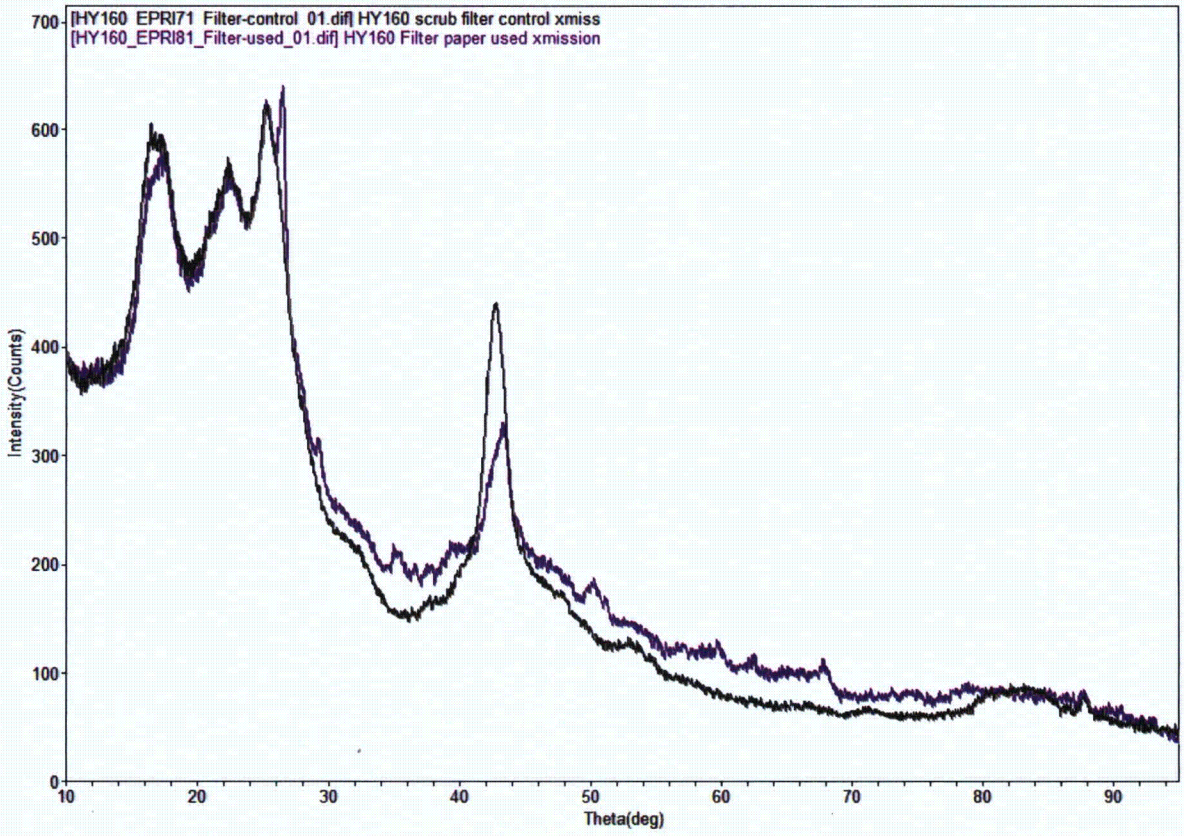

Figure 20: Overlay of data from Filter paper Control (black) and Filter paper Used (purple).

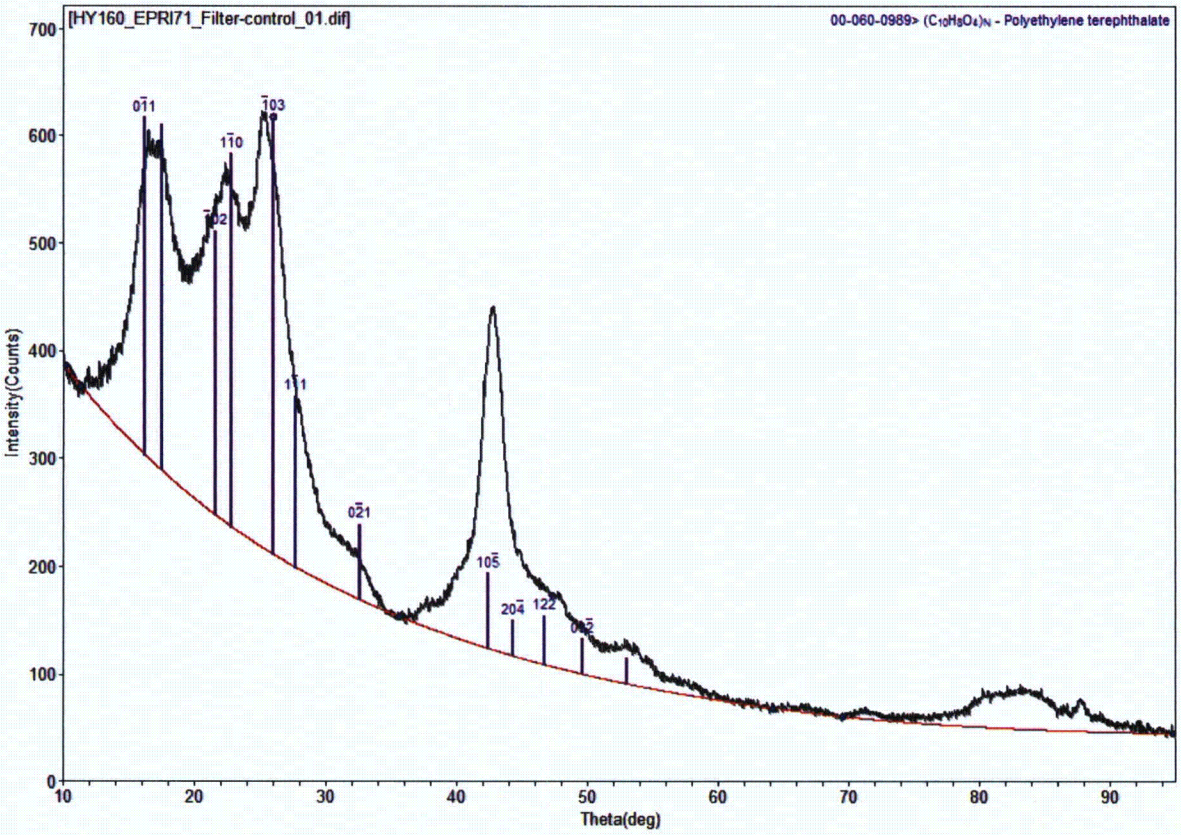

Figure 21: Phase identification of Filter paper Control sample.

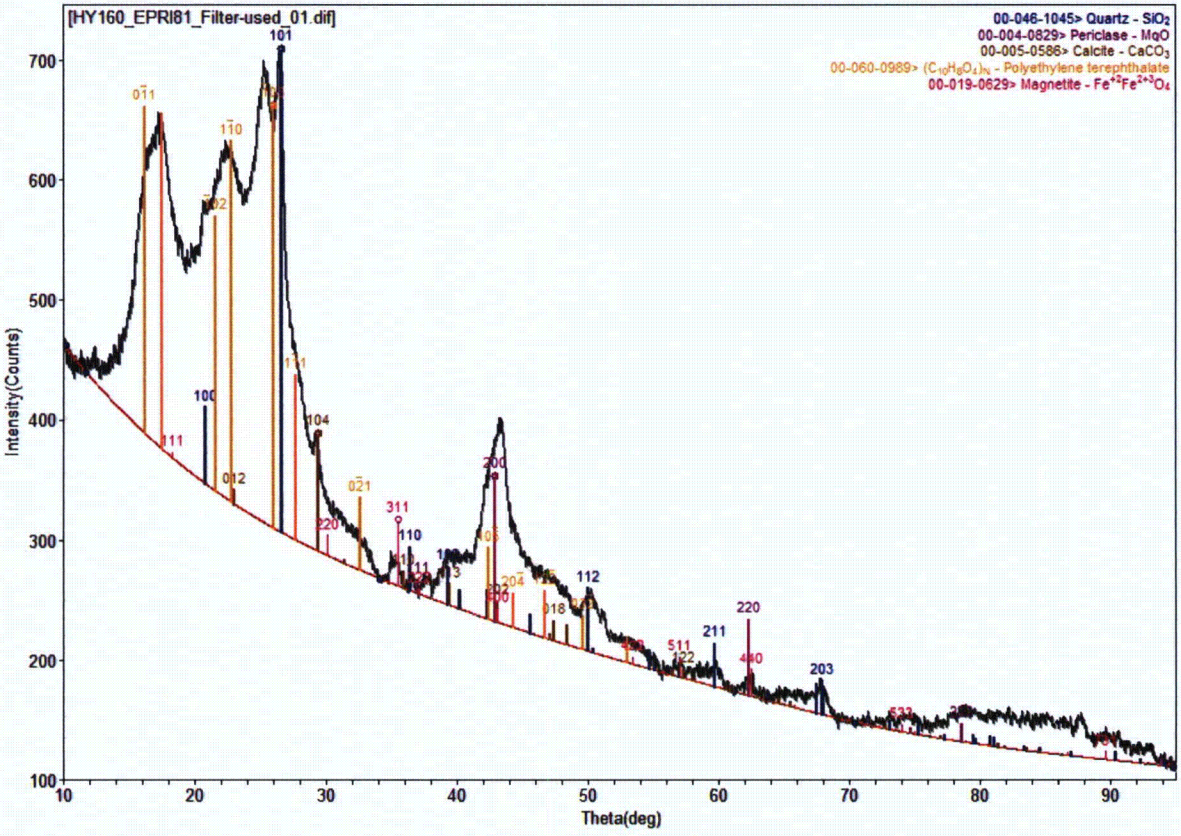

Figure 22: Phase identification of Filter paper Used sample

Appendix

Measurement Uncertainty:

There are two types of uncertainty in XRD analysis; uncertainty in the number of x-ray counts at a particular angle and uncertainty in the diffraction angle. Because the arrival of X-ray quanta in the detector is random with respect to time, the accuracy of X-ray counting rate measurements is governed by the laws of probability. In particular, the size of the one sigma standard deviation in an X-ray measurement is equal to the square root of the number of X-rays counted. A conservative criterion for the detection of a weak peak in a XRD pattern must have amplitude of greater than three standard deviations above background. As a result, the more slowly a measurement is made, the lower the relative standard deviation in the number of counts measured and the more likely is detection of trace diffraction peaks. If X-ray data is acquired at a constant speed, the relative standard deviation for the major diffraction peaks in a pattern will be on the order of a few percent or less while the relative standard deviation for the weaker peaks in a pattern will be on the order of tens of percent or more. This also implies that the uncertainty in the concentrations of the major phases in a sample will be lower than for the trace phases. Please note that there are a number of sample related factors that can influence peak intensity. These include (but are not limited to): average crystallite size, preferred orientation (texture), strain, and absorption.

Uncertainty in the position of X-ray diffraction peaks is due to both instrumental and sample effects. Instrumental position uncertainty is primarily due to diffractometer misalignment. Repeat measurements of NIST standard reference materials has shown that the maximum positional uncertainty is less than +/- 0.05 degrees 2-Theta and is typically much less than that. Positional uncertainty due to sample effects are related to sample displacement (displacement of the sample surface either above or below the diffractometer focusing circle) and sample transparency (the effect gets larger as the sample matrix becomes more transparent to the incident X-rays. Through careful sample preparation, the uncertainty due to these two sample effects should be less than +/- 0.03 degrees 2-Theta. Please note that in addition to these factors, solid solution effects, where one element is partially substituted for another within a given crystal structure, can produce significant shifts in measured peak positions. Unlike sample and instrumental peak position effects, solid solution effects can result in phase misidentification.